ARMY RESEARCH LABORATORY

Electrical Measurements of Ferroelectric Ceramic Resonators

Arthur Ballato and John Ballato

ARL-TR-436 January 1996

NOTICES

Disclaimers

The findings in this report are not to be construed as an official Department of the Army position, unless so designated by other authorized documents.

The citation of trade names and names of manufacturers in this report is not to be construed as official Government endorsement or approval of commercial products or services referenced herein.

REPORT DOCUMENTATION PAGE

Form Approved
OMB NO. 0704-0188

1. AGENCY USE ONLY *(Leave blank)*	2. REPORT DATE	3. REPORT TYPE AND DATES COVERED
	January 1996	Technical Report

4. TITLE AND SUBTITLE
ELECTRICAL MEASUREMENTS OF FERROELECTRIC CERAMIC RESONATORS

5. FUNDING NUMBERS

6. AUTHOR(S)
Arthur Ballato and John Ballato*

7. PERFORMING ORGANIZATION NAMES(S) AND ADDRESS(ES)
US Army Research Laboratory (ARL)
Physical Sciences Directorate (PSD)
ATTN: AMSRL-PS
Fort Monmouth, NJ 07703-5601

8. PERFORMING ORGANIZATION REPORT NUMBER
ARL-TR-436

9. SPONSORING / MONITORING AGENCY NAME(S) AND ADDRESS(ES)

10. SPONSORING / MONITORING AGENCY REPORT NUMBER

11. SUPPLEMENTARY NOTES
*John Ballato is at Rutgers University, Ceramic Science and Engineering Department, Piscataway, NJ 08855-0909.

12a. DISTRIBUTION / AVAILABILITY STATEMENT
Approved for public release; distribution is unlimited.

12 b. DISTRIBUTION CODE

13. ABSTRACT *(Maximum 200 words)*

Future uses of modern ferroelectrics include thin-film resonant microstructures for timimg, sensing, and actuation. The frequency range of interest extends from nearly DC through the UHF band. At high frequencies especially, it is difficult to obtain precise material parameters from broadband electrical measurements. We have developed highly accurate lumped equivalent networks for these frequencies, for the two canonical cases of thickness- and lateral-field excitation. Measurements on these circuits permit extraction of the complex dielectric, piezoelectric, and elastic parameters of the material. In this report we discuss both traditional and modern electrical network descriptions of piezoelectric resonators; we also treat how they are modified by the conditions of excitation and inclusion of loss mechanisms. The more general networks are then specialized to yield lumped circuit versions tailored to the particular attributes of ferroelectrics: high coupling and moderate loss. A numerical example is worked by means of illustration.

14. SUBJECT TERMS
Piezoelectric resonators and devices; network analyzers; simple thickness modes; lumped circuits

15. NUMBER IF PAGES
73

16. PRICE CODE

17. SECURITY CLASSIFICATION OR REPORT	18. SECURITY CLASSIFICATION OF THIS PAGE	19. SECURITY CLASSIFICATION OF ABSTRACT	20. LIMITATION OF ABSTRACT
Unclassified	Unclassified	Unclassified	UL

Table of Contents

List of Figures

List of Tables

ELECTRICAL MEASUREMENTS OF FERROELECTRIC CERAMIC RESONATORS

Preface

This study originated from the emergence of piezoelectric ceramics as candidates for high frequency, low-cost resonators, particularly for telecommunications applications. It was realized that the current generation of measurement standards were inadequate for the characterization precision required. Accordingly, a new approach to the problem was developed, and is detailed in this report.

Arthur Ballato
U.S. Army Research Laboratory
Physical Sciences Directorate
ATTN: AMSRL-PS
Fort Monmouth, NJ 07703-5601
(908) 427-4308; fax -3733
a.ballato@ieee.org

John Ballato
Rutgers University
Ceramic Science & Engrg
Piscataway, NJ 08855-0909
(908) 445-5566; fax -4545
ballato@ccrxr.rutgers.edu

Abstract

Future uses of modern ferroelectrics include thin-film resonant microstructures for timing, sensing, and actuation. The frequency range of interest extends from nearly DC through the UHF band. At high frequencies especially, it is difficult to obtain precise material parameters from broadband electrical measurements. We have developed highly accurate lumped equivalent networks for these frequencies, for the two canonical cases of thickness- and lateral-field excitation. Measurements on these circuits permit extraction of the complex dielectric, piezoelectric, and elastic parameters of the material. In this report we discuss both traditional and modern electrical network descriptions of piezoelectric resonators; we also treat how they are modified by the conditions of excitation and inclusion of loss mechanisms. The more general networks are then specialized to yield lumped circuit versions tailored to the particular attributes of ferroelectrics: high coupling and moderate loss. A numerical example is worked by means of illustration.

Introduction

Modern ferroelectric materials are being developed for a variety of mixed-effect microdevices that utilize the elastoelectric coupling stemming from the piezoeffect. These devices will be required to be uniform in their behavior to an extent unimagined in the past; this, in turn, necessitates the ability to characterize and measure precisely the material properties of the substances from which they are fashioned. The properties in question are the dielectric, piezoelectric, and elastic constants; the measurements are electrical in nature, and the characterization requires highly accurate equivalent electrical networks, valid over a wide frequency range, to describe the physical processes involved. Traditional equivalent circuits suffer from a variety of shortcomings that, e.g., prevent adequate resonator characterization for the purpose of extracting material coefficients, as well as use of electronic frequency-temperature compensation in oscillator (TCXO) applications. The network descriptions presented subsequently are consequences of the piezoelectric nature of poled ferroelectrics. We begin with a brief discussion of the effect and its uses. This is followed by a consideration of traditional equivalent circuit models and modern immittance measuring instruments. Finally, the new broadband models are introduced and explored, with a numerical example.

Piezoelectric Resonators and Devices

The piezoelectric effect was discovered by the brothers Curie in 1880, and remained a curiosity until the early 1920s when its presence in quartz was utilized to realize crystal resonators for the stabilization of oscillators, thereby launching the field of frequency control.[1] With the introduction of quartz control, timekeeping moved from the sun and stars to small, man-made sources that exceeded astronomy-based references in stability. Since then, devices based on piezoelectricity have expanded dramatically in application. The quartz resonator has continued to evolve to become a device capable today of precision one million times greater than the original, and serves as well as the "flywheel" in atomic frequency standards, which make frequency the most accurate entity known.[2]

Piezoelectric devices are additionally used as transducers in applications from telephone speakers to sonar arrays; a newer and rapidly burgeoning area of utilization is the integral incorporation of mechanical actuation and sensing microstructures into electronic chips. These microelectromechanical structures/systems (MEMS) promise signal sensing, processing, and outputting features unattainable by exclusively electronic/photonic means.[3-5] In many traditional applications, applied voltages conform to the norms for electronic circuits; accompanying mechanical displacements are then usually nanometers or less. Newer configurations available today for actuators often have much larger amplitudes at comparable voltages. For high frequency stabilization and control, the configuration of choice is the laminated plate, where thin-film lamina of ferroelectric ceramics or piezoelectrics such as aluminum nitride or zinc oxide serve as the resonant membrane, or where they are used to drive piezoelectrically inert layers of silicon.[6-12] Figure 1 shows examples of modern piezoresonator structures.

One of the most appealing aspects of piezoelectricity for modern applications is the compelling immediacy and simplicity of the transduction mechanism. Micro- and nano-electronics are built upon the behavior of charged species subjected to electric fields; the extreme miniaturization of these structures is owed in large measure to their ability to take on a capacitor-like form.[13] Bulky inductors are eliminated, and thin, planar electrodes introduce the electric fields to operate the circuits. These fields also provide the forces required to drive mechanical motions in a piezoelectric device. Elastic field/mechanical considerations are therefore incorporated into the operations of modern electronic components in a clean, efficient, and very direct manner, by making use of the voltages resident on the chips, via the piezoeffect.

Devices such as MEM structures provide otherwise unavailable capabilities yet are embedded in microelectronic circuitry. The full utility of these components cannot be attained until their behavior is accurately characterized in terms compatible with their operating environment, viz., with admittance matrices, and realized as equivalent electrical networks. This portion of the work is currently in an early stage of development for MEMS devices in general. In the present paper we make use of lossy plate resonator configurations and determine the proper network equivalents from which precise material constant values may be ascertained.

It is interesting to note that, in the 19th Century, when mechanics reigned supreme, luminaries like Kelvin and Maxwell "explained" light phenomena in terms of mechanical models such as coupled gyroscopes.[14,15] Today, electromagnetism and electronics reign, and the art of mechanics seems in many respects an all-but-forgotten discipline. To present the workings of modern mechanical structures such as microactuators and resonators to the "real world," we now make use of equivalent electrical circuits!

Measuring and Characterizing Equipment

The properties of ferroelectric materials for electronic applications are presently characterized by a variety of modalities.[16] These include Scanning Tunneling Microscopy, Atomic Force Microscopy, Electron Microscopy (SEM, TEM, STEM), X-Ray (Synchrotron, XRF, PIXE), Surface (AES, XPS, SIMS, RBS, GDMS, TDMS), and Spectroscopic Techniques (Raman, NMR, ESR). Relatively little attention has been given to determinations of phenomenological characteristics of these substances by modern, computer-driven automatic network analyzer and similar, smart instrumentation metrology; this is briefly discussed below. These instruments are becoming increasingly available for relatively modest capital investments, and represent an efficient method of parameter extraction.

Network Analyzers

Equivalent circuits of electromechanical systems such as piezoelectric resonators serve as a convenient means of describing physics and associated material parameters in a form amenable to engineering treatment and measurement. Today, computer-based electronic instrumentation exists for making highly accurate, broadband measurements of immitance and scattering parameters of networks as function of frequency. When applied to the measurement of ferroelectric

resonators the result is extremely cost-effective. The resonator can be quickly and precisely evaluated as a working device, and its performance judged against specifications to insure reproducibilities at an unprecedented level; the resonator can as well serve instead as a test structure for the accurate determination of the properties of the materials from which it is fashioned. We concentrate on the first aspect in the paper; the second will be treated in a sequel. Regardless of the purpose of the measurements, the method depends upon the availability of accurate circuit models characterizing the physics of the resonating structure.

Once an accurate equivalent circuit is obtained, a programmable network analyzer, e.g., HP 8753C (300 kHz - 3 GHz) or HP 4195A (10 Hz - 500 MHz) can be used to obtain the circuit element values.[17] These are then related to the material values. Alternative measurement methods and techniques, and governing standards are described in the literature.[18-24]

The Butterworth-Van Dyke Circuit

The Butterworth-Van Dyke (BVD) equivalent circuit[25,26] of a resonant system driven by exposure to a capacitive electric field has been exploited for many years to represent piezoelectric resonators.[27-34] The traditional BVD circuit is given in Fig. 2a. A distinction must, however, be made according to the direction of the exciting field; the distinction is represented by the differences in Figs. 2a and 2b. These will be considered in a later section.

One of the best expositors of the use of equivalent circuits, and their applications to both microscopic and macroscopic physics and material science problems was Prof. von Hippel.[27,28] He was also an exponent of having people of differing technical disciplines able to translate freely between the terminology and techniques of physics, engineering, and material science. We seek here to foster this same facility by the application of electric circuits to the determination of material coefficients and performance parameters of ferroelectric components.

The BVD circuit of Fig. 2a leads to the space curve[32] depicted in Fig. 3, where the real (G_p) and imaginary (B_p) parts of the complex admittance function are plotted against frequency variable, f. A number of resonator critical frequencies are indicated; for example, the resonance, f_R, and antiresonance, f_A, frequencies, which occur at the zero phase points, where the susceptance, B_p, vanishes. These particular frequencies are of considerable importance as they determine such things as bandwidth in filter applications, and the normal frequency-reactance operating range of an oscillator. Projections of the space helix, representing the conductance,

G_p, and susceptance as functions of frequency are used to infer certain of the circuit parameter values. Another associated function, the parallel capacitance, $C_p = B_p/\omega$, is shown in Fig. 4 in normalized form, with C_p/C_0 plotted against $\Omega = \omega\sqrt{(L_1C_1)}$. By measuring the hyperbola constant, and the extrema, the BVD elements may be found. Over the years it has been found that the simple BVD circuit often gives an inadequate representation when high precision measurements are made, particularly with ceramics, but even with quartz resonators.[20,35] For these instances more detailed equivalent networks are invoked. In this paper the extended circuits given stem from more detailed considerations of the exact acoustic transmission line description, which is then recast in lumped parameter form. A list of symbols used, units, and dimensions is contained in Appendix 1.

Simple Thickness Modes

In order to treat our subject without undue complication, we assume that the structure under consideration is a piezoelectric plate resonator having an unbounded lateral extent;[36-41] for all practical purposes this is achieved for the thin-film resonators mentioned earlier, which typically have diameter/thickness ratios of 100 or more. This assumption permits use of a one-dimensional approximation, and leads to simplified expressions for the circuit parameters in terms of the material constants of the structure. In more complicated situations,[42,43] the circuit parameters can be extracted in a similar fashion as well; our purpose here is to introduce improved, yet still not unduly complicated, networks for ferroelectric resonators.

We say that plate resonators execute, in the one-dimensional approximation, simple thickness modes of vibration. These are three in number, one is the thickness extensional mode, the two others are the thickness shear modes; each mode is comprised of a family of harmonics, representing varying numbers of phase reversals along the thickness direction. In this paper we consider one mode of vibration; the extension to three modes is straightforward, as is the treatment of coupling of the simple thickness modes. For these plate modes, it is found[39] that the capacitance ratio, $r = C_0/C_1$, of the BVD circuit is related to the piezoelectric coupling factor, k, by the relation: $r = \pi^2/8k^2$. Appendices 2-4 discuss further the use and meaning of k.

Thickness and Lateral Excitation

A plane acoustic wave traveling in a piezoelectric medium is accompanied by an electric field parallel to the direction of propagation. The field is generated by the wave motion, and exists for all directions of propagation in the case of media of general anisotropy; in media of greater symmetry, the field may not exist for certain directions of travel. In this situation, the waves cannot be transduced by imposed fields along these directions, but it may be that they can be driven by laterally directed fields, if an appropriate piezoelectric constant is present. For thickness modes, the direction of travel is along the thickness of the plate. The usual case of transduction is via a pair of electrodes placed on the major surfaces of the plate, to produce a thickness-directed driving field; this is known as thickness excitation (TE). Driving fields impressed from the side produce lateral excitation (LE). Figure 5 depicts both situations. In the LE case the driving field is orthogonal to the wave-produced field in the thickness direction; this situation is appropriate to the BVD circuit of Fig. 2a. Lateral excitation generally permits greater design latitude because the azimuth angle provides an additional degree of freedom. In ceramics, the thickness direction often coincides with the poling direction, and the lateral direction is, therefore, in the isotropic basal plane where the azimuthal angle is of no consequence. The TE situation, where the driving and wave-produced fields are parallel, is shown by the theory[31,34,39,44-46] to be characterized by the BVD circuit of Fig. 2b; the presence of the negative capacitor is a manifestation of the interaction of the driving and wave-produced fields. Thickness excitation is the overwhelmingly predominant form of excitation for piezoelectric plates.

In Fig. 6 the BVD circuits for LE and TE are contrasted. It is seen from the figure that the capacitance ratios r and r' differ by unity. A number of important electrical attributes, e.g., the frequency difference (f_A - f_R), of the networks, are related to the capacitance ratio. Depending upon the size of the piezocoupling factor, k, the use of the traditional BVD network of Fig. 2a (pertinent to the LE case), when the circuit of Fig. 2b is called for (in the usual case of TE), can result in a significant error. This will be seen in greater detail in a later section when a ferroelectric ceramic is used as an example. For now, consider the case of a poled ceramic where k = 51%. From the relation given above, $r = \pi^2/8k^2$, we find that r = 4.74, and r' = 3.74; the difference is greater than 20%, and is therefore quite significant. For a low coupling substance such as AT-cut quartz, where k = 8.80%, r and r' differ by only 0.6%; this is frequently of no consequence.

In Fig. 7 is plotted the reactance of a resonator of a high-coupling material versus frequency for both TE and LE methods of excitation. The relative shift in resonance and antiresonance frequencies in the two cases is readily apparent. Resonance for LE coincides with the TE antiresonance. The effect diminishes with the square of the harmonic, as does the pole-zero separations; this is a consequence of the diminution of effective piezocoupling with overtone.

Exact Lossless Network

Synthesis of the network exactly realizing Y_{in}, the input admittance of a plate resonator executing simple thickness modes, discloses that the individual circuit elements can be given simple interpretations in terms of the physical processes within the mechanically vibrating structure. This leads to analog circuit descriptions of piezoresonators. The complete analog network for the TE case is shown in Fig. 8. The transmission line[47] represents propagation of acoustic waves within the piezoelement. Extension to the case of the composite resonator[48,49] is shown in Fig 9. The network representation follows by inspection because of the modular nature of the circuit parts. Composite resonators are important for determining the material coefficients of nonpiezoelectric materials, and as substrates for thin-film resonators (Fig.1b). It is seen in Fig. 8 that the circuit accommodates electrode mass deposited on the major surfaces of the plate. In the figure the electrode is considered to be thin enough that acoustic wave propagation effects therein can be neglected, and the effect of mass loading wholly ascribed to inertia, which is represented by an inductor at each mechanical port.[50-53]

If the electrode mass loadings on each surface of the plate are equal, the circuit structure of Fig. 8 is completely symmetric, and it may be bisected. The result is seen in Fig. 10. A switch has been added as well, to depict the effect on the circuit of changing from TE to LE. Exact expressions for the input admittance, Y_{in}, of a single excited mode in the one-dimensional approximation, when driven in TE and LE, are:

$$Y_{in}(TE) = j\,\omega\,C_0 / [1 - k^2 T(X)]\,; \qquad Y_{in}(LE) = j\,\omega\,C_0\,[1 + k^2 T(X)]$$

where $T(X) = \tan(X)/(X)$, and $X = \kappa h$. The parameter $\kappa = \omega/v$ is the acoustic wavenumber. Piezoelectric transformer turns ratio, n, appearing in Fig. 10, is found from the relation $n^2 = (eA/2h) = 2\,C_0\,k^2\,f_1/Y_0$; see Appendix 1.

Inclusion of Loss[54-64]

The exact circuit of Fig. 8 is for the lossless situation. We may include the phenomenological effects of loss by two simple expedients. Internal friction within the piezo material is accounted for by making the elastic stiffness complex: $c^E \rightarrow c^* = c^E + j\omega\eta$; the imaginary part is the acoustic viscosity term.[58] This has the effect of making the velocity and wavenumber complex, and leads, in the lumped BVD description, to the presence of the R_1 term. The second provision is for dielectric and ohmic losses. We make the dielectric permittivity complex: $\varepsilon^S \rightarrow \varepsilon^* = \varepsilon' - j\varepsilon''$,[27] and combine ohmic and dielectric loss terms; the total effect is additive, so that the total effective σ is the ohmic conductivity σ plus the dielectric losses, $\omega\varepsilon''$. In the traditional BVD circuit these losses appear as a shunt resistor across the static capacitor C_0; (this can be thought of as a lossy capacitor C*). When the LE version of the BVD circuit is taken, the further addition of the shunt resistor constitutes the ceramic resonator equivalent circuit almost universally used at low frequencies.[35] Viscous and dielectric mechanisms are separately depicted in Fig. 11. The motional time constant is $\tau_1 = R_1C_1 = \eta/c$, where c is the lossless piezoelectrically stiffened elastic stiffness for the mode in question (Appendix 4). The "static" time constant is $\tau_0 = R_0C_0 = \varepsilon'/(\sigma + \omega\varepsilon'')$, which reduces to $\tau_0 = \varepsilon'/\sigma$ in the DC limit. Both τ_1 and τ_0 are real numbers.

In general, both ε' and ε'' are functions of frequency, while $\varepsilon'(\omega)$ and $\varepsilon''(\omega)$ are themselves interrelated by the Cauchy-Riemann equations. In such a case, the network for C_0^* is a parallel connection of a real C_0 and a real G_0, both of which are functions of frequency. Alternatively, depending upon the frequency variation (Cole-Cole relaxation, resonance, etc.), the circuit might be given a more complicated topological form, but with elements having frequency-invariant values. A variation of ε^* with frequency also adds to the dispersion in the acoustic transmission line that arises from the lossy stiffened elastic stiffness. Additional details are contained in Ref. [65].

Lumped Circuits

Passage from the distributed transmission line description to lumped parameters is accomplished by using the partial fractions expansion of the tangent function describing the transmission line,[29] as shown in Fig. 12. Loss is included by making the argument of the tangent function complex, as described earlier. The individual partial fractions then each have lumped

network equivalents as series RLC circuits, and represent the harmonic plate resonances.

The bisected, exact, transmission line circuit model characterizing a lossy plate resonator is shown in Fig. 13. Included here is the extension to the case where the electrode is of a thickness where its wave transmission time cannot be neglected, and the electrode must itself be represented by a transmission line. The figure shows the presence of ohmic and dielectric conductivities modeled by the shunt conductance $G_0 = 1/R_0$, as in the BVD case. Of particular note is the presence of a negative G_0 shunting the negative C_0 of the TE circuit; the negative G_0 and C_0 arise in the lossy case for the same reason as the negative C_0 in the lossless case: the interaction of the driving and wave-produced fields.

When one simplifies Fig. 13 appropriately, one obtains the network of Fig. 14, the new high frequency TE resonator equivalent circuit pertinent to high coupling ceramic, and other ferroelectric materials. For LE, one simply short-circuits the negative elements to arrive at the appropriate network topology. As regards the numerical circuit values pertinent to the two excitation types, we note that values of k for TE and LE are mutually independent, stemming from different piezoelectric coefficients; generally, the electrode geometry is also different, and therefore the two types of piezoelectric driving are represented not only by different circuit topologies, but also by different numerical values. The simplifications necessary to yield Fig. 14 from the distributed analog network are the following:

1) a single resonant harmonic is retained, and modeled by R_M, L_M, C_M; M is an odd number representing the harmonic.

2) the effect of all other harmonics is subsumed into another capacitor, C_R, shunting the R_M, L_M, C_M branch.

3) electrode inertia is modeled by an inductor L_e.

The more accurate circuit of Fig. 14, or the simpler version of Fig. 2c for the situation when C_R can be neglected, is to be contrasted with the network[66-69] usually given for ceramic resonators; viz., an LE BVD with shunt G_0. If necessary to expand the frequency measurement regime to more than one harmonic, the circuit of Fig. 14 may be augmented by the placement of additional series RLC arms shunting that shown, with a concomitant decrease in the value of C_R.

Circuit Element Values

We assume a thickness-excited (TE) piezo resonator of thickness 2h, coated with coextensive electrodes of area A, mass density ρ_e, and thickness h_e on the major plate surfaces. The plate is of mass density ρ; complex dielectric permittivity and total effective conductivity in the thickness direction are ε^* and σ, effective piezoelectric constant is e, and the stiffened elastic constant and viscosity governing the modal velocity and attenuation are denoted by c and η. The requisite values of ε^*, σ, e, η and c are obtained from the material tensor schemes by straightforward methods.[39,44]

In terms of these quantities, and the definitions in Appendix 1, the circuit elements of Fig. 14 are, to our level of approximation:

$C_0 = \varepsilon' A/2h$ $\qquad$ $R_0 = 1/G_0 = \tau_0/C_0$

$C_M = 8 k^2 C_0 /M^2\pi^2$ $\qquad$ $C_R = C_1(\pi^2/8 - 1/M^2)$

$L_M = h^2/2v^2C_0 k^2$ $\qquad$ $L_e = \mu h^2/v^2C_0 k^2 = 2\mu L_M$

$R_M = \tau_1/C_M$ $\qquad$ $k^2 = e^2/\varepsilon' c$

More generally, k^2 is complex, which renders the circuit elements complex. The effects can virtually all be subsumed into the same circuit form with modified values; e.g., L_M and C_M each contain small series resistances, which would be added to R_M.

The curious relation $L_e = 2\mu L_M$ arises for the following reason: mechanical displacement along the thickness direction is sinusoidal, with antinodes at the plate surfaces; an electrode mass lumped at the surface has twice the influence of equivalent mass distributed throughout the thickness because the latter must be weighted by the square of the distribution function.

Ferroelectric Materials, Properties, and Preparation

References [70]-[85] give data on the measured constants of many ferroelectric materials, as well as various properties and methods of preparation. In Fig. 15 is shown a qualitative depiction of the loci occupied by various classes of piezoelectric materials in the quality factor vs capacitance ratio plane. Ceramics occupy a unique and, from a

measurement standpoint, a somewhat troublesome position, possessing very small r values (high coupling factors) and low to moderate Q values. Because of this position, loss considerations are very important, as is the distinction between TE and LE methods of excitation, and, consequently, use of the appropriate equivalent network.

Tables I, II, and III provide the matrices of the permittivity, piezoelectric coefficient, and elastic stiffness for materials in crystal class 6mm, which includes the piezoelectric ceramics, discussed in Appendix 5. Values of σ and η for ferroelectrics in general, and piezoelectric ceramics in particular, are quite scarce in the literature. This may be at least partially attributable to high variability from the lack of sufficient reproducibility in manufacture; the existence of wide variations in loss with temperature, and hysteretic effects may also be responsible for the dearth of these data. Part, at least, of the reason is due to the use of improper or inaccurate equivalent circuit representations by which to characterize these substances. This results in circuit element values that are functions of frequency, and which cannot be related in an obvious and reproducible manner to material parameters.

Numerical Example

We give as an example the circuit parameters and electrical input behavior of a thin-film, thickness-mode ceramic resonator as might be fabricated by sol-gel,[76,85] MOCVD, or laser ablation methods for operation in the VHF-UHF frequency bands. The material chosen is a modified lead titanate.[83] Piezoelectrically stiffened, lossless acoustic velocity is $v = 4400$ m/s; piezocoupling is $k = 51\%$; and dielectric constant in the thickness direction is $\varepsilon^T_{33}/\varepsilon_0 = 263$. We choose specifically a fundamental mechanical response frequency of $f_1 = 250$ MHz; the resonator thickness required is $2h = v/2f_1 = 8.8$ μm. Mass density is taken as $7.52\ 10^3$ kg/m^3. To obtain the permittivity ε^S, necessary to calculate C_0, one would compute $\varepsilon^S_{33} = \varepsilon^T_{33} - e_{33}d_{33} - 2e_{31}d_{31}$. This follows from the relation $\Delta\varepsilon = ed'$ in Appendix 3 applied to substances with transverse isotropy, using the entries in Table II. Since values of e_{31} and e_{33} were not published in Ref.[82], we make the reasonable approximation that $\varepsilon^S \approx \varepsilon^T_{33}(1-k^2)$. This yields $\varepsilon^S \approx 194.59\ \varepsilon_0 \approx 0.7399\ \varepsilon^T_{33} \approx 1.723$ nF/m. The piezo-transformer turns ratio squared is therefore $n^2 \approx 0.842$. We also assume a viscous (or motional) time constant τ_1 of value $\tau_1 = 10^{-12}$ s (loss one hundred times greater than quartz); this is presently unattainable at VHF/UHF, but is anticipated with future advances in material science. A value of total σ (conduction plus dielectric loss) of 10^{-7} S/m is used in the calculations, corresponding to a static time constant, $\tau_0 \approx \varepsilon^S/\sigma$, of 17.23 ms.

We assume also a square electrode patch on each surface of the thin film with dimensions 1 mm by 1 mm by 250 nm. The electrode area is thus $A = 10^{-6}$ m^2, and the width-to-plate-thickness ratio is 1 mm/8.8μm ≈ 114, so the one-dimensional approximation is valid. The acoustic (mechanical) impedance of the ceramic for this particular mode is $Z_0 = A \rho v \approx 33.09$ mechanical ohms (kg/s).

Assuming further that the electrode is of aluminum, with mass density, ρ_e of 2.70 10^3 kg/m^3, the normalized mass loading μ = (electrode mass per unit area/resonator mass per unit area) = $\rho_e h_e/\rho h$ = (2.70x250nm)/(7.52x4.4μm) ≈ 2.04%. Because the acoustic velocity in the electrode is roughly of the same magnitude as that in the ceramic, this is also very nearly the ratio of the acoustic lengths of the electrode and plate in the thickness direction. Because μ is small, it is therefore permissible to substitute a lumped inductor L_e for the transmission line representing the electrode; see Fig. 13. Traditional treatments of mass loading[50-53] show that the normalized mass loading approximates closely the ensuing frequency lowering due to the electrode mass; more accurate results are reported in Ref. [39]. In our case, $\mu = \Delta f/f_1 \approx 2.04\%$, or, since f_1 = 250 MHz, the mass loaded frequency of the purely mechanical resonance is reduced to 244.9 MHz; we shall see that this is indeed the effect of the inductor L_e, representing the mass loading. For the purposes of comparison, equal-thickness electrodes of chromium (ρ_e = 7.19 10^3 kg/m^3; $\mu \approx 5.45\%$), and of gold (ρ_e = 19.32 10^3 kg/m^3; $\mu \approx 14.61\%$), will also be simulated.

The above data permit us to calculate, using the formulas given earlier, the parameters associated with the equivalent network of Fig. 14; these are given, to an accuracy consistent with our other approximations, as follows:

$C_0 \approx 195.8$ pF; $k^2 C_0 \approx 50.93$ pF
$R_0 = 1/G_0 = 8.8\ 10^7$ ohm
$L_e \approx$ 0.401 nH (aluminum)
$\approx$ 1.07 nH (chromium)
$\approx$ 2.87 nH (gold)

For M = 1 (fundamental harmonic),
$C_M = C_1 \approx 41.3$ pF
$C_R \approx$ 9.65 pF; $C_M + C_R \approx 50.95$ pF
$R_M = R_1 \approx 1/41.3$ ohm
$L_M = L_1 \approx 9.82$ nH

Figure 16a shows broadband simulations of the input admittance $|Y_{in}|$ as functions of frequency, using the new, advanced equivalent circuit for electrodes of gold, chromium, and aluminum, showing the effects of differing values of the mass loading parameter, μ; the curves for G_p are very similar to those of $|Y_{in}|$. Fig. 16b shows the input capacitance C_p versus frequency, for aluminum electrodes; the corresponding extrema are given in Table IV. These values are to be compared with those in Table V, computed for the situation where the electrode is of negligible mass. It is seen that the primary effect is a diminution of the critical frequencies.

In Table VI are given the resonance and antiresonance frequencies (defined as the zeros of the C_p function), for a number of electrode substances of differing mass loading (μ) values. The resonance frequencies correspond closely with those of the admittance maxima of Fig. 16a. The last column of Table VI is instructive, as well as of considerable practical importance. The frequency difference (f_R - f_A), is associated with the bandwidth of filters, and with the inductive (operating) region of resonators. It is determined jointly by three factors: piezocoupling, loss, and mass loading. For a lossless resonator having our assumed material and geometrical parameters, without electrode mass loading, the fractional frequency difference $(f_A - f_R)/f_1$ is $[\sqrt{(1+1/r)} - 1] \approx 10.04\%$. Addition of loss increases this to $\approx 11.78\%$; this is found from the first entry in the last column of Table VI. Mass loading decreases the fractional difference slightly, by only $\approx 2.81\%$ per percent μ. To a good approximation, the f_A (i.e., purely mechanical) frequencies may be obtained from the relation $f_A = (1 - \mu) f_1$.

The foregoing has considered the case of thickness excitation. To examine lateral field excitation, we assume that the lateral coupling coefficient is also 51%. In the interest of direct comparison, we assume that 2.04% mass loading is present as well, although LE units typically are devoid of coatings on their major faces. Dielectric coatings are sometimes used for frequency adjustments, but will in the future be discouraged because of aging effects, and other disadvantages. Table VII displays the results for LE; they are obtained by short-circuiting the $-C_0$ and $-G_0$ elements in the TE network. Comparison with Table IV discloses that the responses for LE are reduced in magnitude; this follows from the relations in Fig. 6; because the LE capacitance ratio is larger than for TE, the effective coupling is diminished, and the responses made weaker. The largest effect is to increase the critical frequencies above the TE values. Only the presence of loss reduces the LE frequencies below $f_1 = 250$ MHz.

Table VIII gives the results when both C_R and L_e are set equal to zero; this corresponds to zero mass loading plus neglect of all harmonics except the fundamental. The Table IX results retain the finite aluminum mass loading, but again have $C_R = 0$. Table X through Table XVII list the results for eight different parameter conditions (G_p = maximum, etc.), when the five circuit variations discussed above ($C_R = 0$, etc.) are made.

Table XVIII through Table XX give the resonance, antiresonance, and fractional difference frequencies for aluminum, chromium, and gold electrodes, respectively. For those two circuit conditions having $L_e = 0$, the mass loading vanishes, and the corresponding frequencies in all three tables are seen to agree, as they must. Table XXI provides the susceptance and capacitance slopes at the inflection points of the corresponding functions. Table XXII shows the frequencies where the admittance is maximum for the complete circuit of Fig. 14, and for four circuit fragments.

Behavior at Low Frequencies

Very often measurements are made at low frequencies, typically 1 kHz, in order to infer values for the shunt resistor R_0, and the dissipation factor D_f. This latter factor is arbitrarily defined as the quotient (G_p/B_p) at 1 kHz, and is often set equal to the reciprocal of a quality factor, Q'. While qualitative inferences result, the notion of using such measurements is at best ambiguous, and must be treated with some care. The resonator quality factor, Q, is best regarded instead as the quantity $Q = \sqrt{(L_M/C_M)}/R_M$; this depends solely on the elements of the motional arm, is independent of frequency, and helps determine the vibrator characteristics of the unit near the resonance frequency. As an example of the difficulties that may otherwise arise, consider the result of using measurements at 1 kHz to fix a value of R_0. At this frequency the input capacitance is $C_p \approx 264.67$ pF, and the $Q' \approx 166.9$. Therefore, $R_0 = Q'/(2\pi f C_p) \approx 100.4$ MΩ, not 88 MΩ, the constant value approached in the DC limit. Defining Q' as (B_p/G_p) results in a frequency dependent value which approaches zero (and D_f becomes unbounded) as $f \rightarrow 0$, a situation devoid of practical significance.

Table XXIII gives the values of $Q' = (B_p/G_p)$ and $D_f = 1/Q'$ evaluated at 1kHz for the complete circuit of Fig. 14, and for four circuit fragments.

In the DC limit, moreover, one must distinguish carefully between the lossless and lossy cases when using the TE version of the circuit. In the lossless case, the presence of the $-C_0$ element results in an all-capacitor network having an input admittance of $j\omega C_0/(1 - k^2)$ as $\omega \rightarrow 0$; in the lossy

case, the presence of the $-C_0$ and $-G_0$ elements leads to an admittance of $G_0 + j\omega C_0(1 + k^2)$. In effect, the conductance short-circuits the $-C_0$, and produces the admittance normally associated with lateral excitation. The results agree only in the low-coupling limit; for our example, where $k = 51\%$, the two differ by $k^4 \approx 6.77\%$. Stated in a slightly different way, the input capacitance at a relatively low frequency, but one which is above the relaxation frequency $f \sim 1/2\pi R_0 C_0$, will approximate $C_0/(1 - k^2)$; below the relaxation frequency, C_{in} will approach $C_0(1 + k^2)$. In our case, $1/2\pi R_0 C_0 \sim 9.2$ Hz, and $C_{in} \approx 264.67$ pF at 1kHz and 246.75 at DC.

Simple Ceramic BVD Circuit

The advanced equivalent circuit that has been presented in Fig. 14 and described above stems from the more complicated network of Fig. 13, containing acoustic transmission lines. The network of Fig. 13 represents an exact model for a single, simple thickness mode, and could be augmented to include additional modes. This would have added to the complexity without adding to insight. It could have also been modified to incorporate nonuniform lateral distributions of energy, and "energy trapping" considerations.[39] In these cases, the new circuit of Fig. 14 would retain its lumped topological form, but the element values would be modified. For example, the presence of other harmonics of a single mode type is approximately accommodated in the improved equivalent circuit by the provision of C_R; addition of other modes would simply increase its value in a calculable manner.

Having extracted the advanced network of Fig. 14, the question naturally arises whether one can further reduce it to the form of an elementary BVD circuit (Fig. 2a) with shunt resistance, having frequency-independent elements. This is not possible, as network analytical methods will show. One may, however, construct a rudimentary BVD circuit that "best" describes the complete resonator in some fashion. There are obviously many ways to accomplish this; we give below one such, for the purpose of comparison with the more advanced network of Fig. 14.

We arrive at an equivalent rudimentary (five-element) BVD by making the following assumptions:

- C_0 equals that of the advanced circuit as $f \rightarrow \infty$
- $C_0 + C_1$ equals that of the advanced circuit as $f \rightarrow 0$

These two criteria fix C_0, C_1, and r.

- G_p equals G_0 of the advanced circuit as $f \rightarrow 0$
  This fixes $R_0 = 1/G_0$.

- $(C_{pmax} - C_{pmin}) = Q\,C_1 = F\,C_0$ equals that of the advanced circuit
  This fixes Q, F, E, and the $f_1\,R_1$ product.

- f_1 equals the arithmetic average of the following four values:
  f_{11} = value at which the $f_1\,R_1$ product is satisfied when R_1 is taken as $1/G_{pmax}$ of advanced circuit
  f_{12} = (f at C_{pmax} - f at C_{pmin})/2 of advanced circuit
  f_{13} = f at G_{pmax} of advanced circuit
  f_{14} = f (between C_{pmax} and C_{pmin}) at which C_p of advanced circuit equals C_0.
  This fixes the values of R_1 and L_1.

These four frequency values would be identical if the rudimentary BVD was an adequate equivalent circuit. The above recipe yields the following parameter values:

$R_0 = 88\ M\Omega$; $C_0 = 195.8\ pF$;
$L_1 = 10.70\ nH$; $R_1 = (1/46.38)\ \Omega$; $C_1 = (C_R + C_M) = 50.95\ pF$

A comparison of some pertinent quantities of the advanced and simple lumped networks is given in Table XXIV. The slope of the normalized capacitance curve at the inflection point is equal to -2FQ = -2E, for the simple BVD circuit.[86,87] The table indicates discrepancies from 5% to greater than 20%. Simulations of input conductance and capacitance versus frequency for both the advanced and simple networks are shown in Fig. 17a and b, respectively, in the vicinity of the resonance. It is seen from Fig. 17 that the simple circuit produces curves that are qualitatively similar to those generated by the advanced network, but that the curves are sufficiently divergent not to be adequate for characterizing devices to the extent that will be required by future manufacturing specifications.

A comparison of the curves generated by the advanced network of Fig. 14 with those of the exact transmission line circuit of Fig. 13, shows, by comparison, deviations at the percentage level, and only in the immediate vicinity of f_R, the resonance frequency. Some of the divergence is due to errors in rounding the element values, and some to using only the real parts of the lumped circuit elements; much of the remainder is thought to be due to treating all the nonresonant harmonics on the same footing, as lumped capacitors, instead of RC combinations. The advanced network, without additional modifications, is appropriate and adequate for

specification of the highly accurate and reproducible ceramic resonators of the future.

Conclusion

Novel, lumped electrical equivalent circuits have been derived from transmission line analog networks; these yield accurate results for characterizing highly piezoelectric lossy materials, such as ceramics and other ferroelectrics, for high frequency operation.

Acknowledgment

The authors wish to thank Dr. James T. Stewart for computations relating to the numerical example.

References

[01] W G Cady, *Piezoelectricity*, McGraw Hill, NY, 1946; Dover, NY, 1964.

[02] E A Gerber and A Ballato, eds., *Precision Frequency Control*, Vol. 1 and 2, Academic Press, New York, NY and Orlando, FL, 1985.

[03] G J Knowles, ed., *Active Materials and Adaptive Structures*, Institute of Physics Publishing, Bristol and Philadelphia, 1992.

[04] R E Newnham and G R Ruschau, "Smart electroceramics," J. Am. Ceram. Soc., Vol. 74, No. 3, March 1991, pp. 463-480.

[05] J Bryzek, K Petersen, and W McCulley, "Micromachines on the march," IEEE Spectrum, Vol. 31, No. 5, May 1994, pp. 20-31.

[06] K M Lakin, J S Wang, G R Kline, A R Landin, Y Y Chen, and J D Hunt, "Thin film resonators and filters," IEEE Ultrasonics Symp. Proc., San Diego, CA, October 1982, pp. 466-475. IEEE Catalog No. 82CH1823-4.

[07] J S Wang and K M Lakin, "Sputtered c-axis inclined ZnO films for shear wave resonators," IEEE Ultrasonics Symp. Proc., San Diego, CA, October 1982, pp. 480-483. IEEE Catalog No. 82CH1823-4.

[08] E A Gerber, T Lukaszek, and A Ballato, "Advances in microwave acoustic frequency sources," IEEE Trans. Microwave Theory Tech., Vol. MTT-34, No. 10, October 1986, pp. 1002-1015.

[09] S V Krishnaswamy, "Film bulk acoustic wave resonator technology," IEEE Microwave Theory Tech. Society Newsletter, Number 130, Fall 1991, pp. 21-25.

[10] Y -K Yong, J T Stewart, and A Ballato, "A laminated plate theory for high frequency, piezoelectric thin-film resonators," J. Appl. Phys., Vol. 74, No. 5, 1 September 1993, pp. 3028-3046.

[11] R B Stokes, "X-band thin film acoustic filters on GaAs," IEEE Trans. Microwave Theory Tech., Vol. 41, No. 6/7, June/July 1993, pp. 1075-1080.

[12] K M Lakin, G R Kline, and K T McCarron, "High-Q microwave acoustic resonators and filters," IEEE Trans. Microwave Theory Tech., Vol. 41, No. 12, December 1993, pp. 2139-2146.

[13] US Congress, Office of Technology Assessment, "Miniaturization Technologies," OTA-TCT-514 (Washington, DC: US Government Printing Office, November 1991), 48pp.

[14] W T Kelvin, *Baltimore Lectures on Molecular Dynamics and the Wave Theory of Light*, Cambridge Univ. Press, London, 1904. Lecture I (October 1, 1884), pp. 12-13; Lecture IX (October 8, 1884), pp. 104-105; Lecture X (October 9, 1884), pp. 118-119; and Lecture XI (October 10, 1884), pp. 126-129.

[15] J C Maxwell, *A Treatise on Electricity and Magnetism*, 3rd Ed., 1891, Dover, New York, 1954. See particularly Vol. 2, pp.228 and 431.

[16] J B Wachtman, *Characterization of Materials*, Butterworth-Heinemann, Boston, 1993.

[17] *1994 Test & Measurement Catalog*, Hewlett-Packard Company, Santa Clara, CA, 1993.

[18] "IRE Standards on Piezoelectric Crystals, 1949," Proc. IRE, Vol. 37, No. 12, December 1949, pp. 1378-1395.

[19] "IRE Standards on Piezoelectric Crystals: Determination of the Elastic, Piezoelectric, and Dielectric Constants - The Electromechanical Coupling Factor, 1958," Proc. IRE Vol. 46, No. 4, April 1958, pp. 764-778. IEEE Standard 178.

[20] E Hafner, "The piezoelectric crystal unit - definitions and methods of measurement," Proc. IEEE, Vol. 57, No. 2, February 1969, pp. 179-201.

[21] "IEEE Standard on Piezoelectricity," IEEE Standard 176-1978, IEEE, New York, 55pp.

[22] "IEEE Standard Definitions of Primary Ferroelectric Terms," ANSI/IEEE Standard 180-1986, IEEE, NY, 21pp.

[23] IEC Publication 444: "Basic Method for the Measurement of Resonance Frequency and Equivalent Series Resistance of Quartz Crystal Units by Zero Phase Technique in a π-Network (1973)." ANSI, New York.

[24] IEC Publication 483: "Guide to Dynamic Measurements of Piezoelectric Ceramics (1976)." ANSI, New York.

[25] S Butterworth, "On a null method of testing vibration galvanometers," Proc. Phys. Soc. (London), Vol. 26, 1914, pp. 264-273.

[26] K S Van Dyke, "The electric network equivalent of a piezo-electric resonator," (Abstract), Phys. Rev., Vol. 25, No. 6, June 1925, p. 895.

[27] A R von Hippel, *Dielectrics and Waves*, (1954), MIT Press, Cambridge, MA, 1966.

[28] Ferroelectrics, Vol. 135, Numbers 1-4, 1992. Special Issue on Dielectric Properties of Ferroelectrics on the Occasion of the 94th Birthday of Prof. von Hippel.

[29] M Marutake, "Approximate method of calculating electro-mechanical coupling factor," Proc. IRE, Vol. 49, May 1961, p. 967; Vol. 50, February 1962, pp. 214-215.

[30] D A Berlincourt, D R Curran, and H Jaffe, "Piezoelectric and piezomagnetic materials and their function in transducers," in *Physical Acoustics: Principles and Methods*, W P Mason, ed., Academic Press, NY, 1964, Vol. I, Part A, Chap. 3, pp. 169-270.

[31] H Schüssler, "Darstellung elektromechanischer keramischer Wandler als Dickenscherschwinger mit piezoelektrischer und piezomagnetischer Anregung," Archiv der Elektrischen Übertragung, Vol. 22, No. 8, August 1968, pp. 399-406.

[32] A Ballato, "Resonance in piezoelectric vibrators," Proc. IEEE, Vol. 58, No. 1, January 1970, pp. 149-151.

[33] E Hafner, "Crystal resonators," IEEE Trans. Sonics Ultrason., Vol. SU-21, No. 4, October 1974, pp. 220-237.

[34] A Ballato, "Equivalent networks for piezoelectric resonators and transducers," Proc. 5th European Frequency and Time Forum, Besançon, France, March 1991, pp. 465-473.

[35] B Parzen, *Design of Crystal and Other Harmonic Oscillators*, John Wiley & Sons, New York, 1983, Chapter 3, "Piezoelectric Resonators," pp. 66-122 and 432-436.

[36] H F Tiersten, "Thickness vibrations of piezoelectric plates," J. Acoust. Soc. Amer., Vol. 35, No. 1, January 1963, pp. 53-58.

[37] H F Tiersten, "Wave propagation in an infinite piezoelectric plate," J. Acoust. Soc. Amer., Vol. 35, No. 2, February 1963, pp. 234-239.

[38] T R Meeker, "Thickness mode piezoelectric transducers," Ultrasonics, Vol. 10, No. 1, January 1972, pp. 26-36.

[39] A Ballato, "Doubly rotated thickness mode plate vibrators," in *Physical Acoustics: Principles and Methods*, (W P Mason and R N Thurston, eds.), Vol. 13, Chap. 5. Academic Press, New York, 1977, pp. 115-181.

[40] J F Rosenbaum, *Bulk Acoustic Wave Theory and Devices*, Artech House, Boston and London, 1988.

[41] B A Auld, *Acoustic Fields and Waves in Solids*, 2nd edition, Vol. I and II, R. E. Krieger Pub. Co., Malabar, FL, 1990.

[42] R F Milsom, "Two-dimensional theory of thin-film ZnO resonators on silicon," IEEE Ultrasonics Symp. Proc., San Diego, CA, October 1982, pp. 484-489. IEEE Catalog No. 82CH1823-4.

[43] A Ballato and J G Smits, "Network representation for piezoelectric bimorphs," IEEE Trans. Ultrason. Ferro. Freq. Contr., Vol. 38, No. 6, November 1991, pp. 595-602.

[44] A Ballato, E R Hatch, M Mizan, and T J Lukaszek, "Lateral field equivalent networks and piezocoupling factors of quartz plates driven in simple thickness modes," IEEE Trans. Ultrason., Ferroelec., & Frequency Control, Vol. UFFC-33, No. 4, July 1986, pp. 385-392.

[45] A Ballato, T Lukaszek, M Mizan, and J Kosinski, "Lateral- and thickness-field coupling in zincblende structures," Proc. 41st Annual Frequency Control Symp., May 1987, pp. 325-332. IEEE Catalog No. 87CH2427-3.

[46] A Ballato, "Equivalent circuits for resonators and transducers driven piezoelectrically," Technical Report SLCET-TR-90-12, U. S. Army Laboratory Command, Fort Monmouth, NJ, October 1990, 45pp. AD-A231520.

[47] H J Carlin, "Distributed circuit design with transmission line elements," Proc. IEEE, Vol. 59, No. 7, July 1971, pp. 1059-1081.

[48] W J Price and H B Huntington, "Acoustical properties of anisotropic materials," J. Acoust. Soc. Amer., Vol. 22, No. 1, January 1950, pp. 32-37.

[49] H B Huntington, *The Elastic Constants of Crystals*, Academic Press, NY, 1958, pp. 52-53.

[50] A Ballato, "Apparent orientation shifts of mass-loaded plate vibrators," Proc. IEEE, Vol. 64, No. 9, September 1976, pp. 1449-1450.

[51] H Nowotny and E Benes, "General one-dimensional treatment of the layered piezoelectric resonator with two electrodes," J. Acoust. Soc. Am., Vol. 82, No. 2, August 1987, pp. 513-521.

[52] S J Martin, V E Granstaff, and G C Frye, "Characterization of a quartz crystal microbalance with simultaneous mass and liquid loading," Anal. Chem., Vol. 63, No. 20, 15 October 1991, pp. 2272-2281.

[53] A Ballato, T J Lukaszek, and G J Iafrate, "Subtle effects in high-stability quartz resonators," Ferroelectrics, Vol. 43, Nos. 1/2, 1982, pp. 25-41.

[54] J J Kyame, "Conductivity and viscosity effects on wave propagation in piezoelectric crystals," J. Acoust. Soc. Amer., Vol. 26, November 1954, pp. 990-993.

[55] W P Mason, "Phonon viscosity and its effect on acoustic wave attenuation and dislocation motion," J. Acoust. Soc. Amer., Vol. 32, No. 4, April 1960, pp. 458-472.

[56] R M Glaister, "Measurement of coupling coefficient and Q of low-Q piezoelectric ceramics," British Jour. Appl. Phys., Vol. 11, August 1960, pp. 390-391.

[57] G Arlt, "Resonance-antiresonance of conducting piezoelectric resonators," J. Acoust. Soc. Amer., Vol. 37, No. 1, January 1965, pp. 151-157.

[58] J Lamb and J Richter, "Anisotropic acoustic attenuation with new measurements for quartz at room temperatures," Proc. Roy. Soc. (London), Vol. A293, 1966, pp. 479-492.

[59] J B Thaxter and P E Tannenwald, "Phonon generation, propagation, and attenuation at 70 GHz," IEEE Trans. Sonics Ultrason., Vol. SU-13, No. 2, July 1966, pp. 61-69.

[60] R Holland, "Representation of dielectric, elastic, and piezoelectric losses by complex coefficients," IEEE Trans. Sonics Ultrason., Vol. SU-14, No. 1, January 1967, pp. 18-20.

[61] M G Holland, "Thermal conductivity and ultrasonic attenuation," IEEE Trans. Sonics Ultrason., Vol. SU-15, No. 1, January 1968, pp. 18-27.

[62] W H Robinson and A Edgar, "The piezoelectric method of determining mechanical damping at frequencies of 30 to 200 kHz," IEEE Trans. Sonics Ultrason., Vol. SU-21, No. 2, April 1974, pp. 98-105.

[63] A Ballato, "The fluency matrix of quartz," IEEE Trans. Sonics Ultrason., Vol. SU-25, No. 2, March 1978, pp. 107-108.

[64] G Arlt, U Böttger, and S Witte, "Dielectric dispersion of ferroelectric ceramics and single crystals by sound generation in piezoelectric domains," J. Am. Ceram. Soc., Vol. 78, No. 4, April 1995, pp. 1097-1100.

[65] A Mansingh and M Sayer, "Dielectric response of ferroelectric films," Proc. Ninth IEEE Intl. Symp. Appl. Ferroelec. (ISAF94), The Pennsylvania State University, August 1994, pp. 663-668. IEEE Catalog No. 94CH3416-5.

[66] R Holland and E P EerNisse, *Design of Resonant Piezoelectric Devices*, MIT Press, Cambridge MA, 1969.

[67] H H Schuessler, "Ceramic filters and resonators," IEEE Trans. Sonics Ultrason., Vol. SU-21, No. 4, October 1974, pp. 257-268.

[68] H Schewe, "Piezoelectricity of uniaxially oriented polyvinylidene fluoride," IEEE Ultrasonics Symp. Proc., San Diego, CA, October 1982, pp. 519-524. IEEE Catalog No. 82CH1823-4.

[69] J Söderkvist and K Hjort, "Flexural vibrations in piezoelectric semi-insulating GaAs," Sensors and Actuators A, Vol. 39, 1993, pp. 133-139.

[70] Landolt-Börnstein, Numerical Data and Functional Relationships in Science and Technology, New Series, Group III: Crystal and Solid State Physics, Volumes III/1, 1966; III/2, 1969; III/3, 1969; III/9, 1974; III/11, 1979; III/16a, 1981; III/16b, 1982; III/17a, 1982; and III/29a, 1992. Springer-Verlag, Berlin, New York.

[71] B Jaffe, W R Cook, Jr, and H Jaffe, *Piezoelectric Ceramics*, Academic Press, New York, 1971.

[72] L L Hench and J K West, *Principles of Electronic Ceramics*, John Wiley & Sons, New York, 1990.

[73] E Akçakaya, G W Farnell, and E L Adler, "Dynamic approach for finding effective elastic and piezoelectric constants of superlattices," J. Appl. Phys., Vol. 68, No. 3, 1 August 1990, pp. 1009-1012.

[74] K Han, A Safari, and R E Riman, "Colloidal processing for improved piezoelectric properties of flexible 0 - 3 ceramic-polymer composites," J. Am. Ceram. Soc., Vol. 74, No. 7, July 1991, pp. 1699-1702.

[75] C Z Rosen, B V Hiremath, and R Newnham, eds., *Piezoelectricity*, American Institute of Physics, New York, 1992.

[76] C Livage, A Safari, and L C Klein, "Sol-gel lead zirconate-titanate thin films: effect of solution concentration," Proc. Eighth IEEE Intl. Symp. on Appls. of Ferroelectrics (ISAF '92), Greenville, SC, August 1992, pp. 444-447. IEEE Catalog No. 92CH3080-9.

[77] D J Waller and A Safari, "Piezoelectric lead zirconate titanate ceramic fiber/polymer composites," J. Am. Ceram. Soc., Vol. 75, No. 6, June 1992, pp. 1648-1655.

[78] L F Brown, "Ferroelectric polymers: current and future ultrasound applications," IEEE Ultrasonics Symp. Proc., October 1992, pp. 539-550.

[79] V Sundar and R E Newnham, "Electrostriction and polarization," Ferroelectrics, Vol. 135, 1992, pp. 431-446.

[80] J B Wachtman and R A Haber, eds., *Ceramic Films and Coatings*, Noyes Publications, Park Ridge, New Jersey, 1993.

[81] M L Dunn and M Taya, "Electromechanical properties of porous piezoelectric ceramics," J. Am. Ceram. Soc., Vol. 76, No. 7, July 1993, pp. 1697-1706.

[82] D Tahan, A Safari, and L C Klein, "The preparation of dielectric ($Ba_{0.8}$, $Sr_{0.2}$) Ti O_3 thin films by sol-gel method," Proc. Sixth US-Japan Seminar on Dielectric and Piezoelectric Ceramics, 1993, pp. 47-50.

[83] T Suwannasiri and A Safari, "Effect of rare-earth additives on electromechanical properties of modified lead titanate ceramics," J. Am. Ceram. Soc. Vol. 76, No. 12, December 1993, pp. 3155-3158.

[84] J G Gualtieri, J A Kosinski, and A Ballato, "Piezoelectric materials for acoustic wave applications," IEEE Trans. Ultrason., Ferroelec., and Freq. Control, Vol. 41, No. 1, January 1994, pp. 53-59.

[85] H Schmidt, "The sol-gel process for the synthesis and processing of ceramic powders," Interceram, Vol. 43, No. 2, March 1994, pp. 90, 93.

[86] A Ballato and G R Oliva, Jr, "Admittance bridge determination of quartz vibrator parameters using augmenting immittance elements," IEEE Trans. Instrum. and Meas., Vol. IM-19, No. 2, May 1970. pp. 128-135.

[87] G R Oliva, Jr, and A Ballato, "Quartz vibrator parameter determination by parallel bridge methods," Technical Report ECOM-3121, U. S. Army Electronics Command, Fort Monmouth, NJ, August 1969, 47pp. AD-697110.

APPENDICES

Appendix 1. Units and Dimensions

Field tensors:

Mechanical stress, S	pascal, Pa = newton/meter^2 = N/m^2
Mechanical strain, T	meter/meter = m/m = dimensionless
Electric intensity, E	volt/meter = V/m
Displacement, D	coulomb/meter^2 = C/m^2

Matter tensors:

Mass density, ρ, ρ_e		kg/m^3
Permittivity, ε^T, ε^S		farad/meter = F/m = C/(m-V)
Impermeability, β^T,β^S		meter/farad = m/F = (m-V)/C
Conductivity, σ		siemens/meter = S/m
Piezo constants	e	C/m^2 = N/(m-V)
	d	m/V = C/N
	h	V/m = N/C
	g	m^2/C = (m-V)/N
Elastic stiffness, c^E, c^D		Pa = N/m^2 = J/m^3
Compliance, s^E, s^D		$(Pa)^{-1}$ = m^2/N = m^3/J
Viscosity, η		pascal-second = Pa-s

Network and resonator parameters (subscript "e" = electrode):

Acoustic impedance $Z_0 = A\rho v = 1/Y_0$ $Z_e = A\rho_e v_e = 1/Y_e$	kg/s
Acoustic velocity $v = \sqrt{(c/\rho)}$ $v_e = \sqrt{(c_e/\rho_e)}$	m/s
Acoustic wavenumber $\kappa = \omega/v$ $\kappa_e = \omega/v_e$	m^{-1}
Capacitance, C_0, C_1, C_M, C_R	farad
Capacitance ratio $r = C_0/C_1$	dimensionless
Dissipation factor $D_f = G_p/B_p$, at 1 kHz	dimensionless
Elastic stiffness c, c_e	pascal
Electrode area A	$meter^2$
Electrode thickness (each) h_e	meter
Figure of excellence $E = Q^2/r$	dimensionless
Figure of merit $F = Q/r$	dimensionless

Frequency variables ω, f	hertz = Hz = s^{-1}
Harmonic number, M	odd integer
Inductance, L_1, L_M, L_e	henry
Mass loading parameter, μ	dimensionless
Normalized frequency $\Omega = \omega/\omega_1 = f/f_1$	dimensionless
Piezocoupling factor $k = e/\sqrt{(\varepsilon c)}$	dimensionless
Piezo-transformer turns ratio $n = Ae/(2h)$ $n^2 = 2C_0\, k^2 f_1 Z_0$	N/V = C/m
Plate thickness 2h	meter
Quality factor $Q = [\sqrt{(L_1/C_1)}]/R_1$ $Q' = 1/D_f$	dimensionless
Resistance, R_0, R_1, R_M $R_0 = 1/G_0$	ohm
Series resonance frequency $f_1 = \omega_1/2\pi$	hertz
Series resonance pulsatance $\omega_1 = 1/\sqrt{(L_1C_1)}$	hertz
Surge impedance $z_1 = \sqrt{(L_1/C_1)}$ $= Q\, R_1$	ohm
Time constant $\tau_1 = R_1C_1 = \eta/c$ $\tau_0 = R_0C_0 =$ $\varepsilon'/(\sigma + \omega\varepsilon'') \approx \varepsilon^S/\sigma$	second = s (motional, dynamic) ("static")

Appendix 2. Material Constitutive Equations

Piezoelectricity couples the mechanical stress (T) and strain (S) fields with the electric intensity (E) and displacement (D) fields. Depending on variable choice, four sets of material constitutive relations are defined for the linear case of insulating dielectric materials; these are, in compressed matrix form:

$$[T] = [c^E][S] - [e]'[E]; \quad [D] = [e][S] + [\varepsilon^S][E]$$

$$[T] = [c^D][S] - [h]'[D]; \quad [E] = -[h][S] + [\beta^S][D]$$

$$[S] = [s^E][T] + [d]'[E]; \quad [D] = [d][T] + [\varepsilon^T][E]$$

$$[S] = [s^D][T] + [g]'[D]; \quad [E] = -[g][T] + [\beta^T][D]$$

Because the electric variables [E] and [D] are tensors of rank 1 (i.e., three-dimensional vectors), and the mechanical variables [T] and [S] are tensors of rank two which have been converted to six-dimensional vectors, $[c^E]$, $[c^D]$ and $[s^E]$, $[s^D]$ are (6 X 6) symmetric matrices representing the elastic stiffnesses and compliances at constant E and D; $[\varepsilon^S]$, $[\varepsilon^T]$ and $[\beta^S]$, $[\beta^T]$ are symmetric (3 X 3) dielectric permittivity and impermeability matrices at constant S and T, while [e], [h], [d], and [g] are (3 X 6) piezoelectric matrices. A prime denotes transpose. Alternative formulations, using the electric polarization vector [P] in place of [D], are sometimes used, particularly in electrooptic applications; piezoelectric polarization [a] and [b] matrices are then used. The matrix brackets [ ] are omitted in Appendix 3 and 4 for simplicity.

The crystallographic point-group symmetry elements completely determine the form and symmetries of the elastic, piezoelectric, and dielectric matrices that appear in the constitutive relations. The specific values of the individual components result, of course, from the particular substance considered.

Appendix 3. Matter Tensor Identities

The material constants are interrelated as follows:

$\varepsilon^+ \beta^+ = c^* s^* = I$, where + is T or S, * is E or D, and I = unit matrix, and

$$e = \varepsilon^S h = d c^E; \quad d = \varepsilon^T g = e s^E; \quad h = \beta^S e = g c^D; \quad g = \beta^T d = h s^D$$

In addition to these multiplicative identities, difference relations exist between the dielectric quantities at constant stress and at constant strain and between the elastic constants at constant electric field and at constant displacement; the following are found:

$$(c^D - c^E) = h' e = e' \beta^S e = h' \varepsilon^S h$$

$$(s^E - s^D) = g' d = d' \beta^T d = g' \varepsilon^T g$$

$$(\varepsilon^T - \varepsilon^S) = e d' = e s^E e' = d c^E d'$$

$$(\beta^S - \beta^T) = g h' = h s^D h' = g c^D g'$$

These relations show that the presence of piezoelectricity modifies the elastic and dielectric constants, that the mechanical (elastic) conditions must be specified for dielectric quantities, and that electric conditions must be specified for elastic quantities. To obtain an order of magnitude estimate of the size of the effect, we may neglect the matrix nature of the above equations and treat them as scalars. Then, using the symbol Δ to represent differences, we have, from the first difference relation:

$$(\Delta c/c) = e \beta^S e/c = e^2/(\varepsilon c) = k^2,$$

and similarly for the other relations. Thus the fractional differences are determined by dimensionless combinations of elastic, piezoelectric, and dielectric constants. We call each combination the square of a quantity, k, known as a piezoelectric coupling factor. See Appendix 4.

Appendix 4. Electromechanical Coupling Factors

Electromechanical coupling factors k ($0 \leq k < 1$) are dimensionless measures of efficacy of piezoelectric transduction, and are far more important than the piezoelectric constants taken by themselves. They appear in considerations of bandwidth and insertion loss in transducers and signal processing devices, in location and spacing of critical frequencies of resonators, and in electrical/mechanical energy conversion efficiency in actuators. For high frequency plate resonators, coupling factors have the generic form $k = e / \sqrt{(\varepsilon c)}$; for low frequency bar and rod vibrators, the form becomes $k = d / \sqrt{(\varepsilon s)}$; alternative forms using the "h" and "g" piezo parameters are used as well. These quantities are also called piezocoupling factors.

The passage of an acoustic wave in a piezoelectric medium produces a self-generated electric field that alters the effective elastic coefficient determining the wave velocity. The effective elastic coefficient is called the stiffened elastic constant c; it is computed from the c^E, e, and ε^S tensors; treating these as scalars for the sake of simplicity, c takes the form $c = c^E +$

e^2/ε^S; ($c^E + j\omega\eta + e^2/\varepsilon^*$ when loss is considered). The stiffened value $c = \rho v^2$ may thus be expressed in terms of the piezoelectric coupling factor, k, as $c = c^E/(1-k^2)$.

Appendix 5. The Ferroelectric Point Groups

Piezoelectric ceramics, such as lead zirconate titanate ($Pb(Ti,Zr)O_3$), are solid solutions comprised of microscopic crystallites, each of which is ferroelectric; the material originally is macroscopically isotropic at all temperatures because of the random orientations of the crystallites. When cooled through the Curie point in the presence of a static electric field (a process called "poling"), the domains are preferentially oriented and frozen into a configuration where the body is macroscopically piezoelectric. It remains isotropic perpendicular to the field axis, but the isotropy is destroyed in the parallel direction. The result is cylindrical polar symmetry (transverse isotropy), represented by the symbol ∞mm; as far as the elastic, piezoelectric, and dielectric matrices are concerned, the schemes of coefficients are identical to those for the class 6mm. In fact, for all tensors up to and including rank five, the schemes of coefficients are identical to the corresponding class 6mm schemes; one may differentiate transversely isotropic substances from 6mm crystals by measuring higher-order effects, e.g., third-order elastic constants (tensor of rank six).

All ferroelectrics must be members of one of the pyroelectric classes: 1, 2, m, mm2, 4, 4mm, 3, 3m, 6, and 6mm. Above the Curie point, most (but not all) ferroelectrics belong to one of three classes: 222 (e.g., Rochelle salt), 4bar 2m (e.g., potassium dihydrogen phosphate, KDP), and m3m (e.g., $BaTiO_3$). In the ferroelectric state, most of the practically important compounds likewise fall into three classes: 4mm, 3m, and mm2.

Tables I, II, and III give, respectively, the permittivity matrix [ε], the [e] form of the piezoelectric matrix, and the elastic stiffness matrix [c] for piezo class 6mm (e.g., transversely isotropic, poled polycrystalline ceramics such as lead zirconate titanate as well as single- or poly-crystal AlN and ZnO, used in thin-film form on Si for MEMS devices).

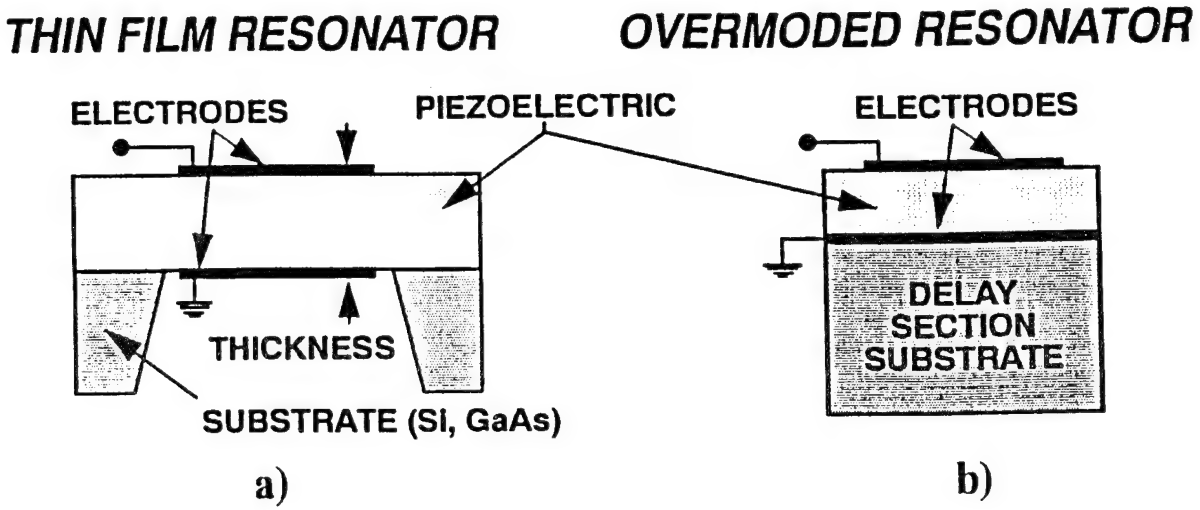

Figure 1. One- and two-port resonator configurations for microwave frequencies.

a). A thin-film fundamental mode resonator supported at its periphery by a substrate.

b). An overmoded resonator consisting of a thin-film piezoelectric transducer fabricated on a low-loss substrate having reflecting surfaces.

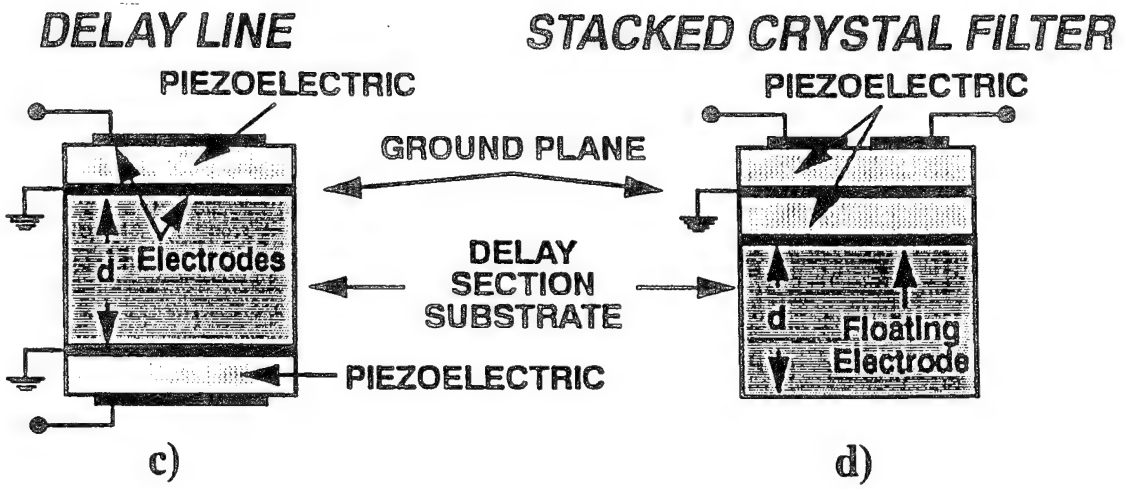

Figure 1. One- and two-port resonator configurations for microwave frequencies.

c). A two-port resonator in the form of a delay line weakly coupled to the source and load to provide a large standing wave and high Q response.

d). A stacked crystal filter having two layers of piezoelectric films. Two stacked single sections are shown connected in series so as to bring the output electrode to the surface. (After Ref. [6]).

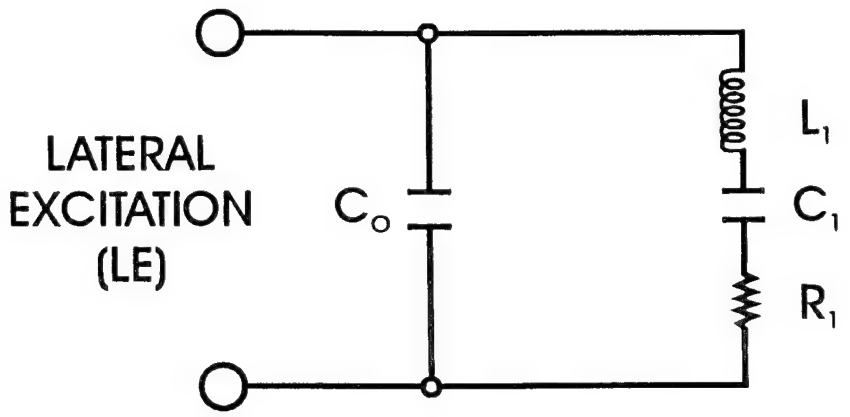

Figure 2. Resonator equivalent networks. a). The traditional Butterworth-Van Dyke (BVD) circuit for lateral excitation (LE) of a plate resonator.

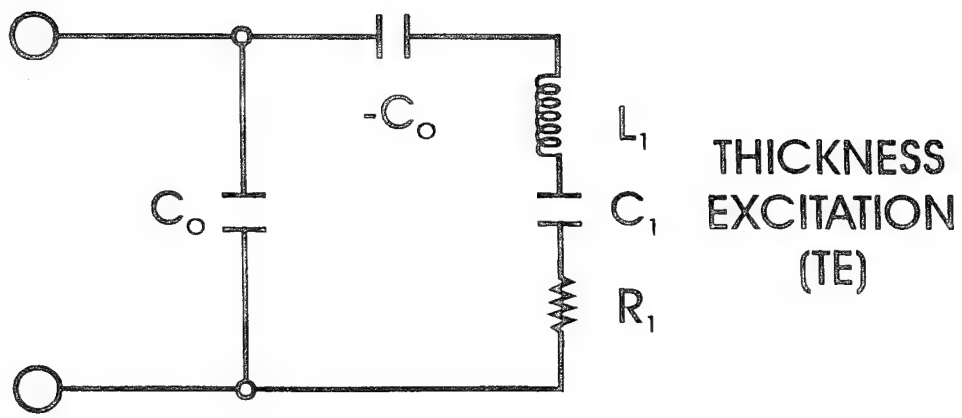

Figure 2. Resonator equivalent networks. b). The BVD circuit for thickness excitation (TE) of a plate resonator. The negative capacitor arises from the interaction between the self-generated electric field of the acoustic wave and the imposed driving field.

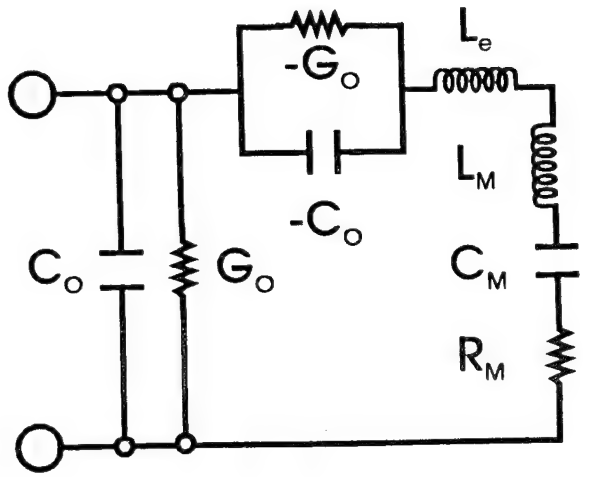

Figure 2. Resonator equivalent networks. c). Extension of the TE version to accommodate dielectric/ohmic losses and electrode inertia.

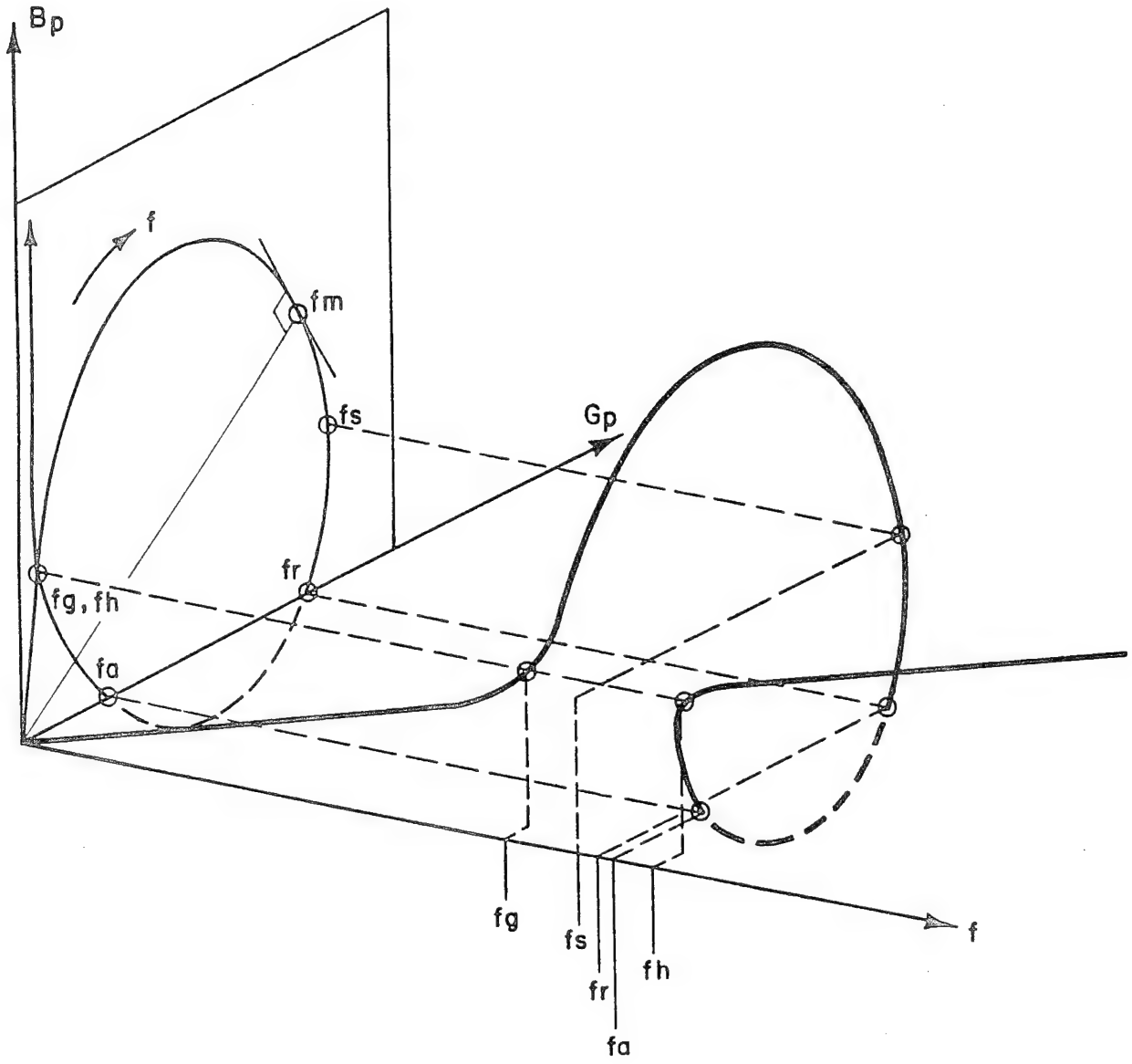

Figure 3. Depiction of real (G_{-p}) and imaginary (B_p) parts of input admittance of the simple four-element BVD circuit as function of frequency. In the vicinity of the resonance loop, the network response becomes a sensitive function of frequency.

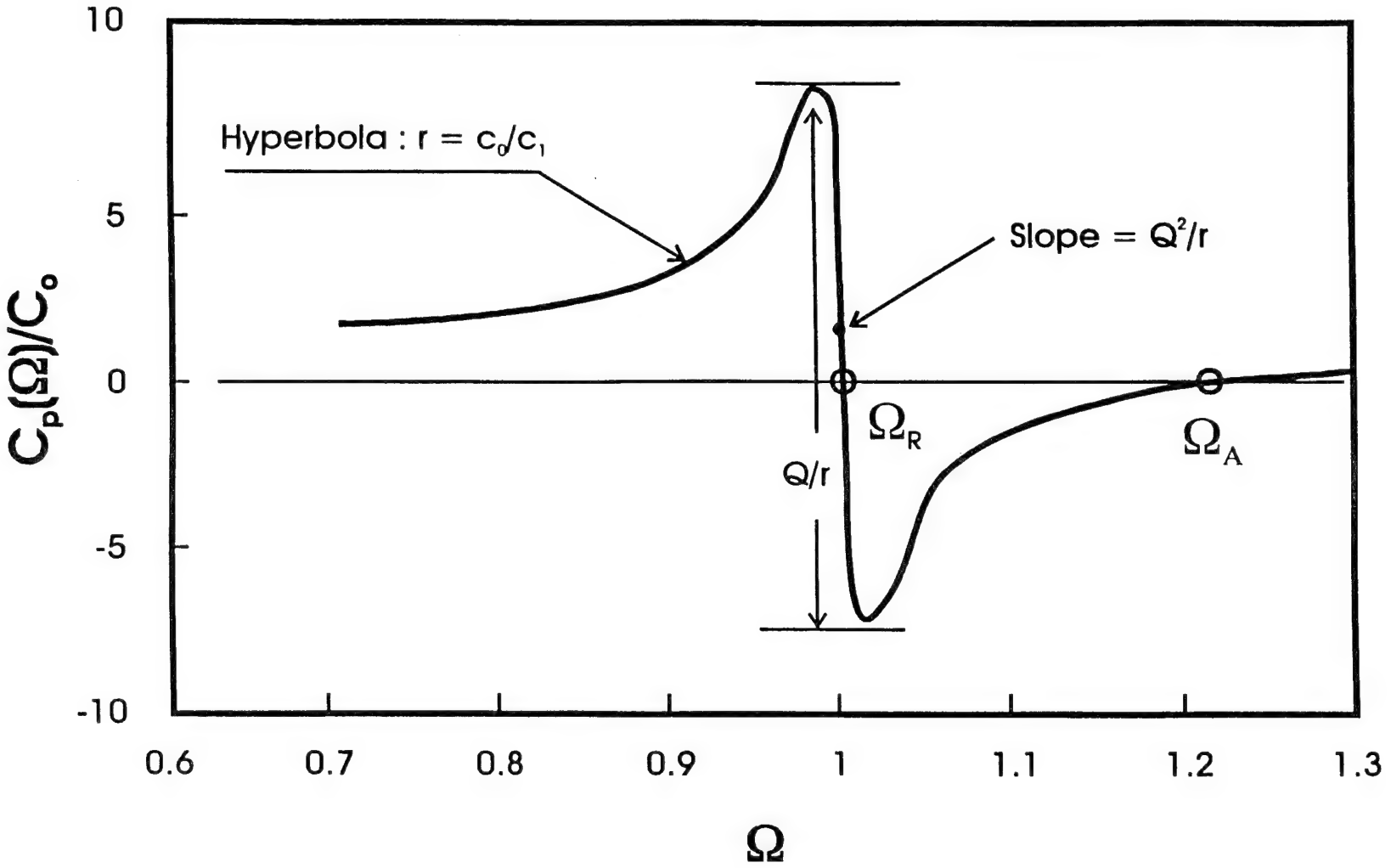

Figure 4. Normalized input capacitance of the BVD circuit of Fig. 3 as function of frequency, normalized to the resonance frequency. The hyperbolic region determines the capacitance ratio, r. The quality factor, Q, may be found from either the extrema of the curve, or from the slope maximum in the region of anomalous dispersion.

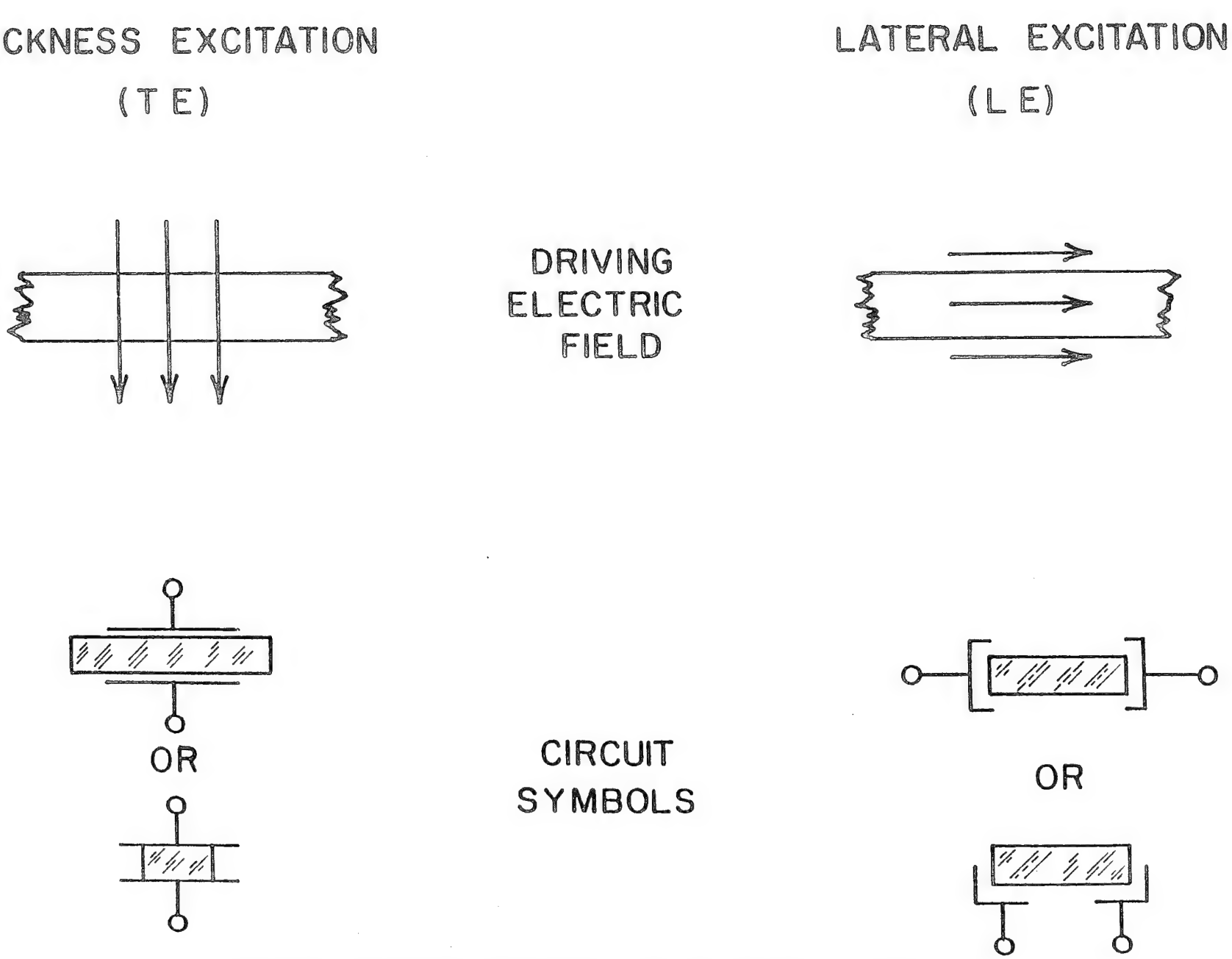

Figure 5. Schematic depiction of the two canonical means of excitation of plate resonators, thickness excitation (TE) and lateral excitation (LE). Circuit symbols are also shown.

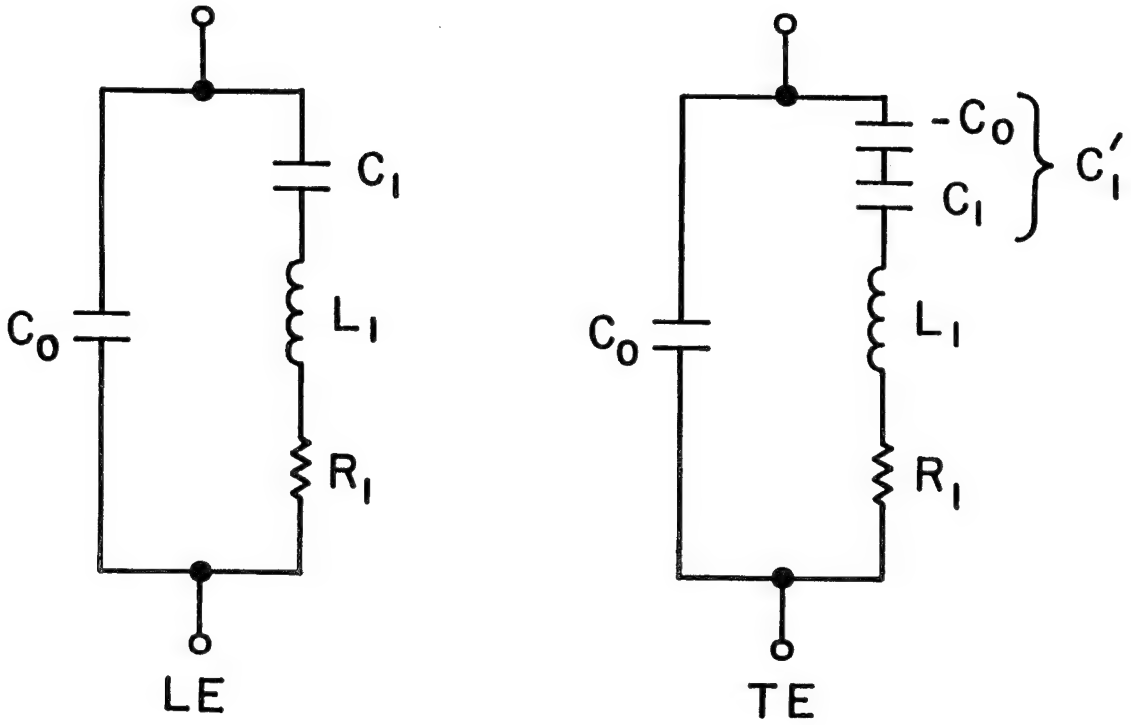

$$C_1' = C_0 C_1 / (C_0 - C_1)$$

$$r = C_0 / C_1$$

$$r' = C_0 / C_1'$$

$$\boxed{r' = r - 1}$$

Figure 6. Capacitance ratios for LE and TE BVD representations. The cases differ by unity. For low-coupling materials such as quartz, the difference is usually negligible; for high-coupling ceramics, the difference is appreciable.

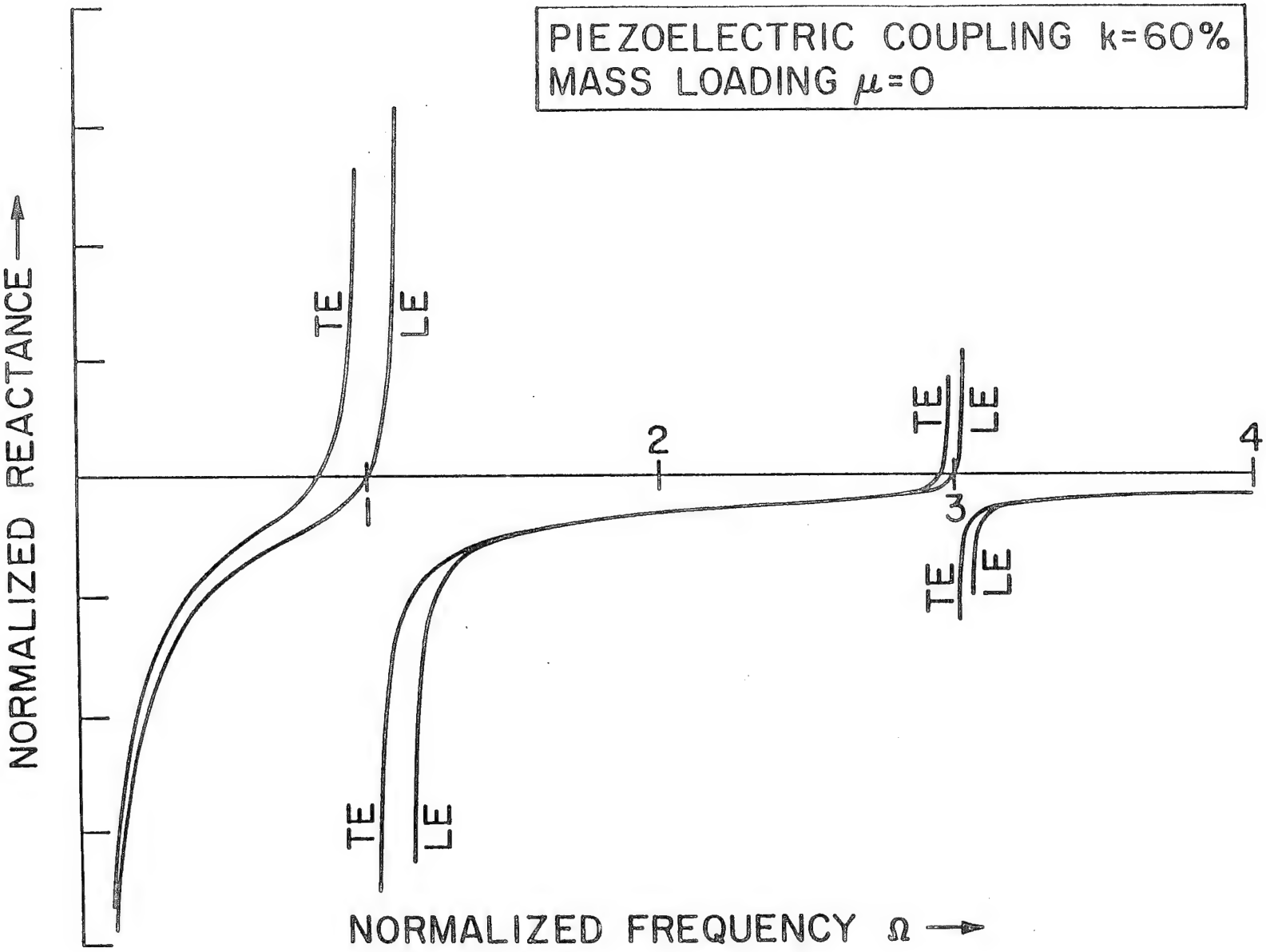

Figure 7. Reactance versus frequency, normalized to the fundamental resonance, for the LE and TE BVD circuits, with piezocoupling of 60% and no electrode mass loading. The reactance zero for LE coincides with the pole of TE, and the pole-zero separation diminishes quadratically with harmonic for both TE and LE.

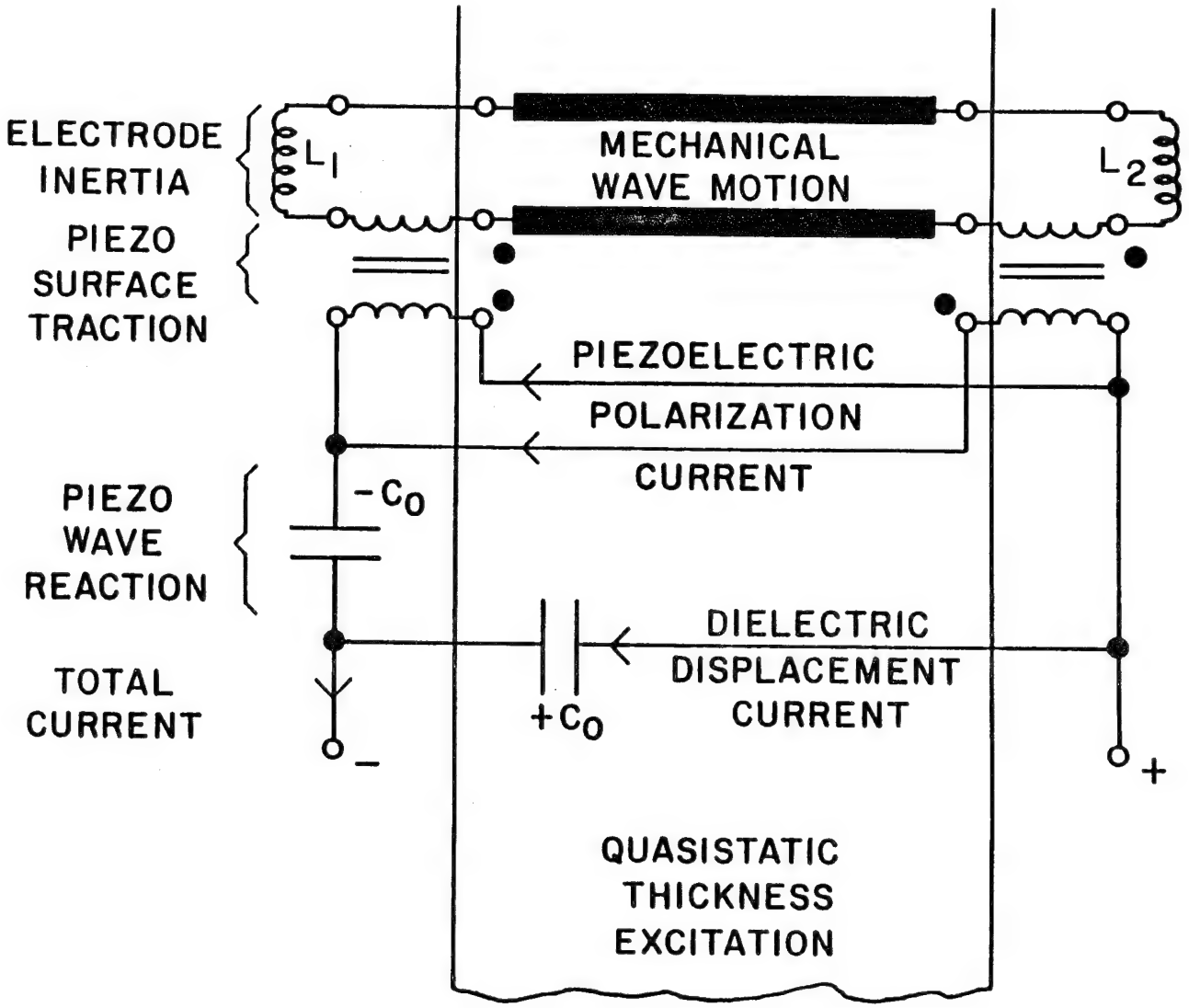

Figure 8. Exact, distributed network for TE of a piezoelectric plate, with physical correspondences indicated. The acoustic transmission line models the mechanical wave motion in the plate. At the plate surfaces are lumped forces of piezoelectric traction, represented by the piezo transformers, and electrode mass inertia, represented by the inductors L_1 and L_2.

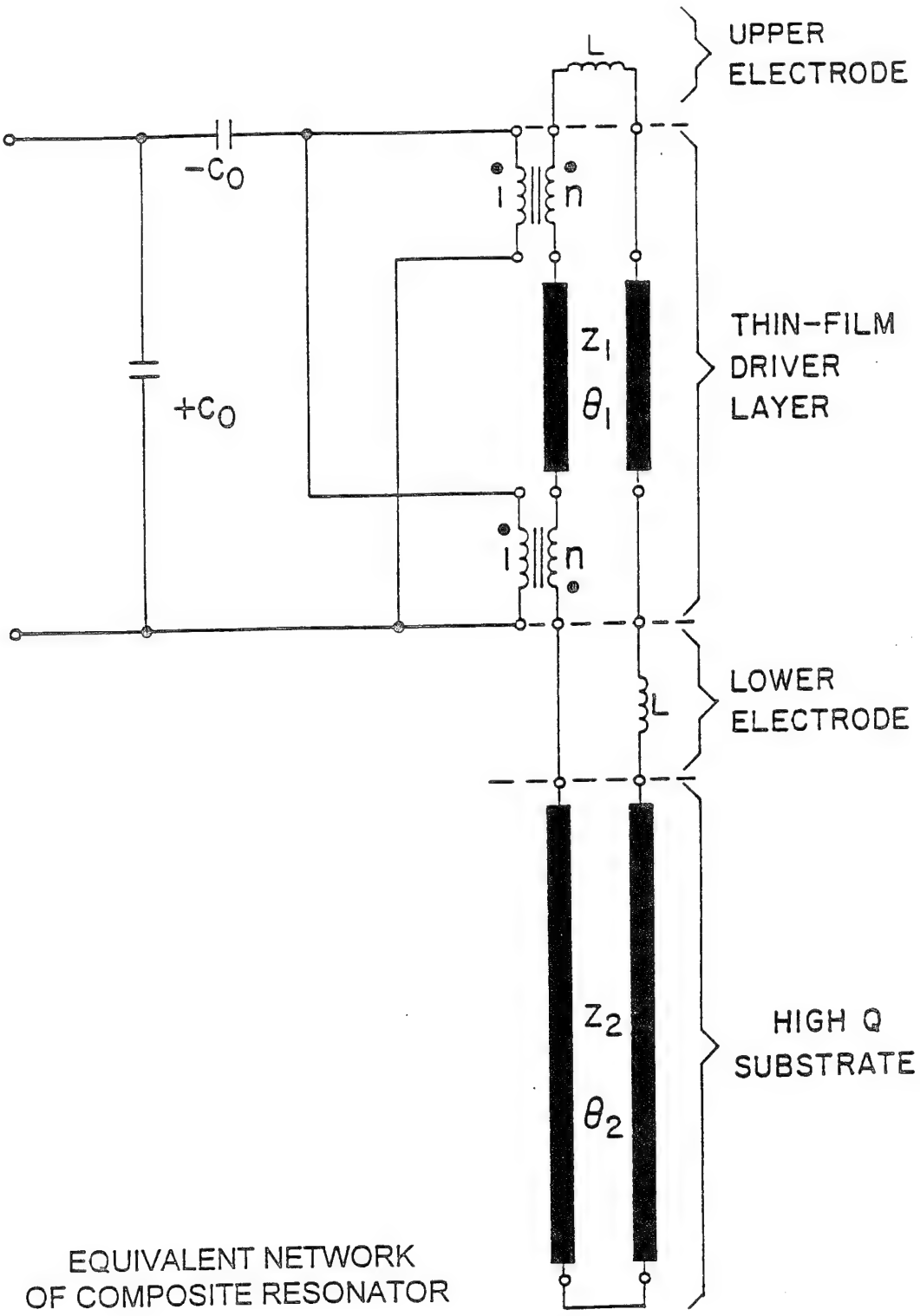

Figure 9. The circuit of Fig. 8 altered to model a composite resonator. A second acoustic transmission line represents the nonpiezoelectric substrate, and is connected to add to the surface tractions at one mechanical port of the driving resonator. This circuit can be used to model thin piezo-films applied on a substrate, or to determine the properties of piezoelectrically inert materials. Z_1, Z_2 are the mechanical impedances of the media; θ_1, θ_2 are the corresponding phase "distances" of each structure (wavenumber times length).

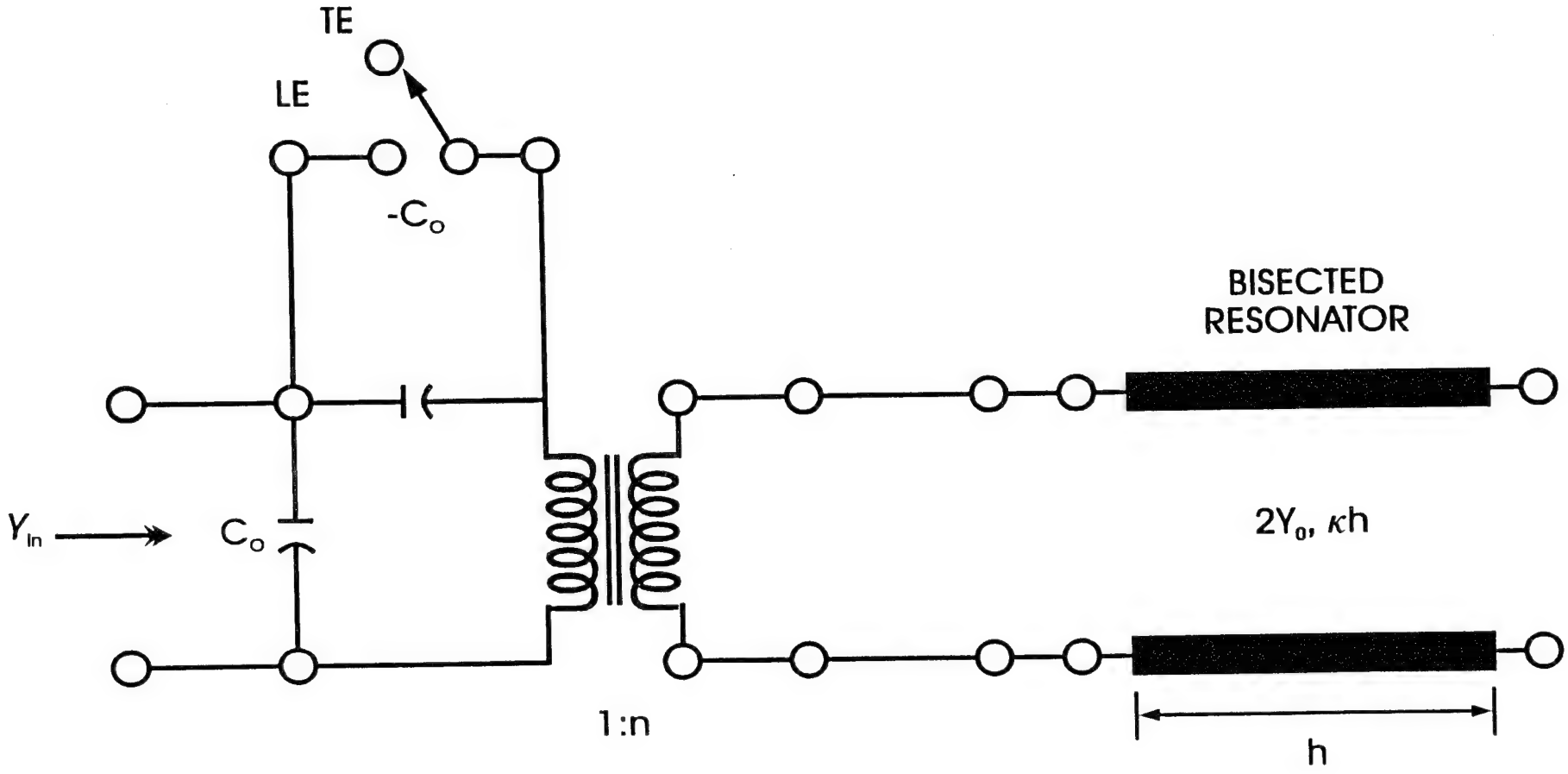

Figure 10. The symmetry of Fig. 8 permits the transmission line to be bisected and the two halves to be combined. The results, excluding the inductive effect of electrode inertia, are portrayed in Fig. 10, along with the formulas for input admittance of the TE and LE cases.

TIME CONSTANTS

TYPE	BVD CIRCUIT

ELASTIC VISCOSITY

$$c^* = c^E (1 + j\omega\tau_1)$$

$$\tau_1 = \eta / c^E = R_1 C_1$$

(motional time constant)

R_1 generally also includes mount and ambient losses.

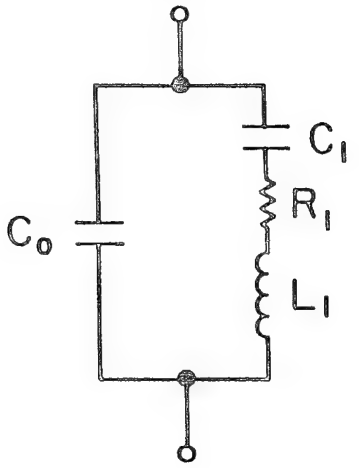

ELECTRONIC CONDUCTIVITY

$$\epsilon^* = \epsilon^S (1 + 1/j\,\omega\tau_0)$$

$$\tau_0 = \epsilon^S / \sigma = R_0 C_0$$

(static time constant)

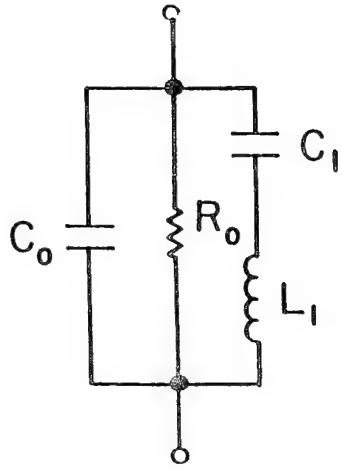

Figure 11. Static and motional time constants, representing loss mechanisms, and appearance in BVD circuits. Internal friction in the resonator material is represented by R_1 in series with the motional L_1C_1 arm, and calculated from the material viscosity. Losses arising from ohmic conductivity and dielectric loss are subsumed into an effective conductivity, and appear as a shunt resistor $R_0 = 1/G_0$.

$$Y_{in} = j\,Y_0 \tan\left(\frac{\omega h}{v}\right)$$

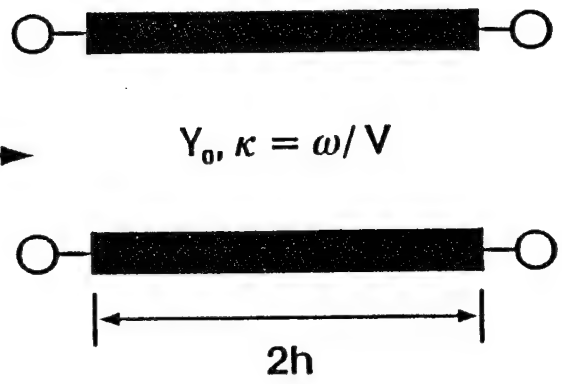

$$\tan Z = \sum_{\substack{M \\ \text{odd}}}^{\infty} \frac{8Z}{M^2\pi^2 - 4Z^2} = \frac{\sin(2x) + j\sinh(2y)}{\cos(2x) + \cosh(2y)}$$

(PARTIAL FRACTIONS)

$$Z = x + jy = \frac{\omega h}{v}$$

Figure 12. Input admittance of an open-circuited transmission line. Its distributed nature is reflected in the transcendental tangent function describing its behavior. The tangent function expansion in partial fractions about its singularities is valid for all nonsingular points, and is used to arrive at a description of the transmission line with loss in terms of a sequence of RLC lumped elements, one for each singularity, i.e., harmonic resonance.

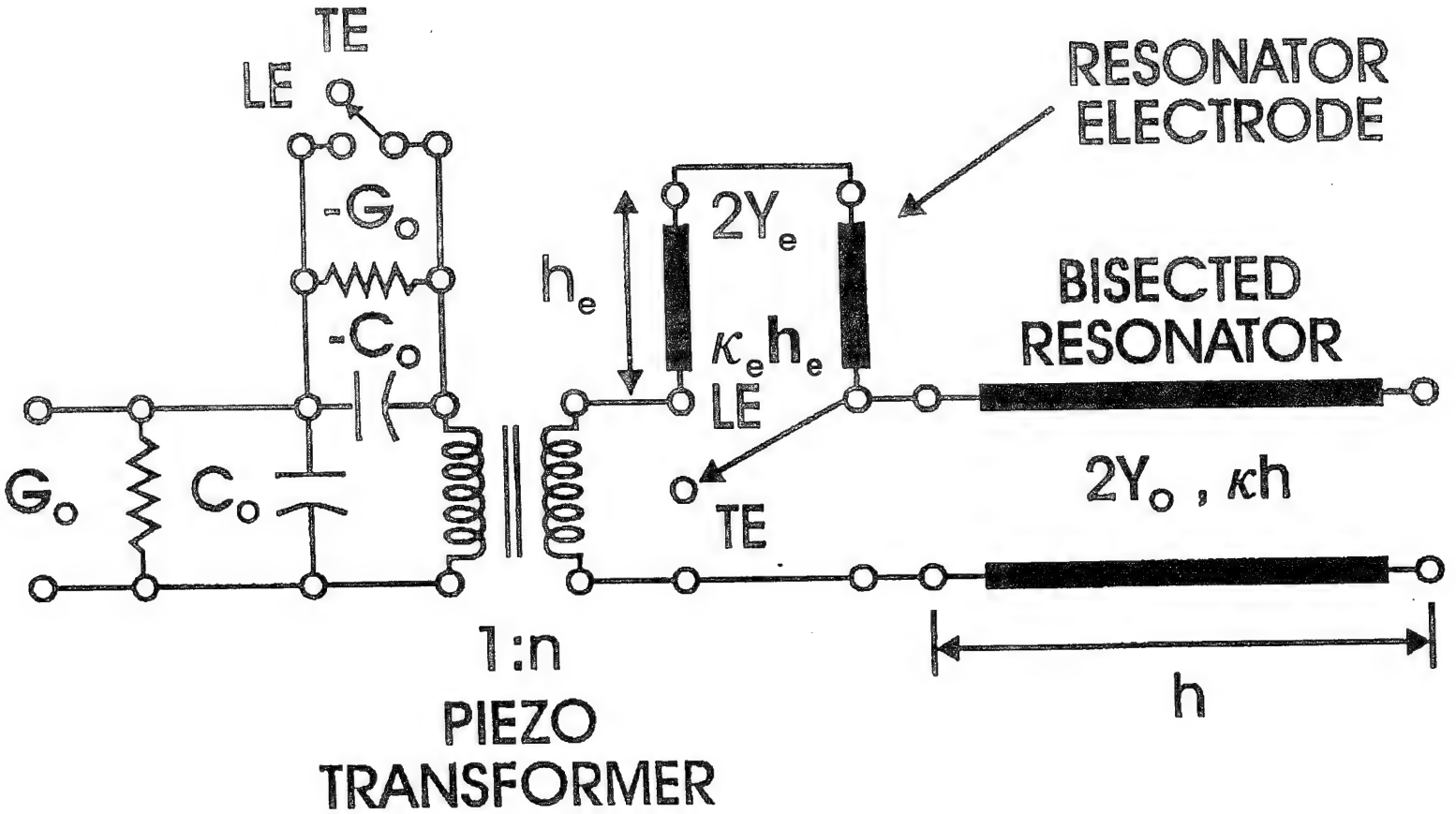

Figure 13. Exact network description of a bisected, thickness-excited plate resonator with electrodes of such a thickness that wave transmission effects cannot be neglected. It is usually the case that the electrode can be reduced to a lumped inductor representing a purely inertial effect.

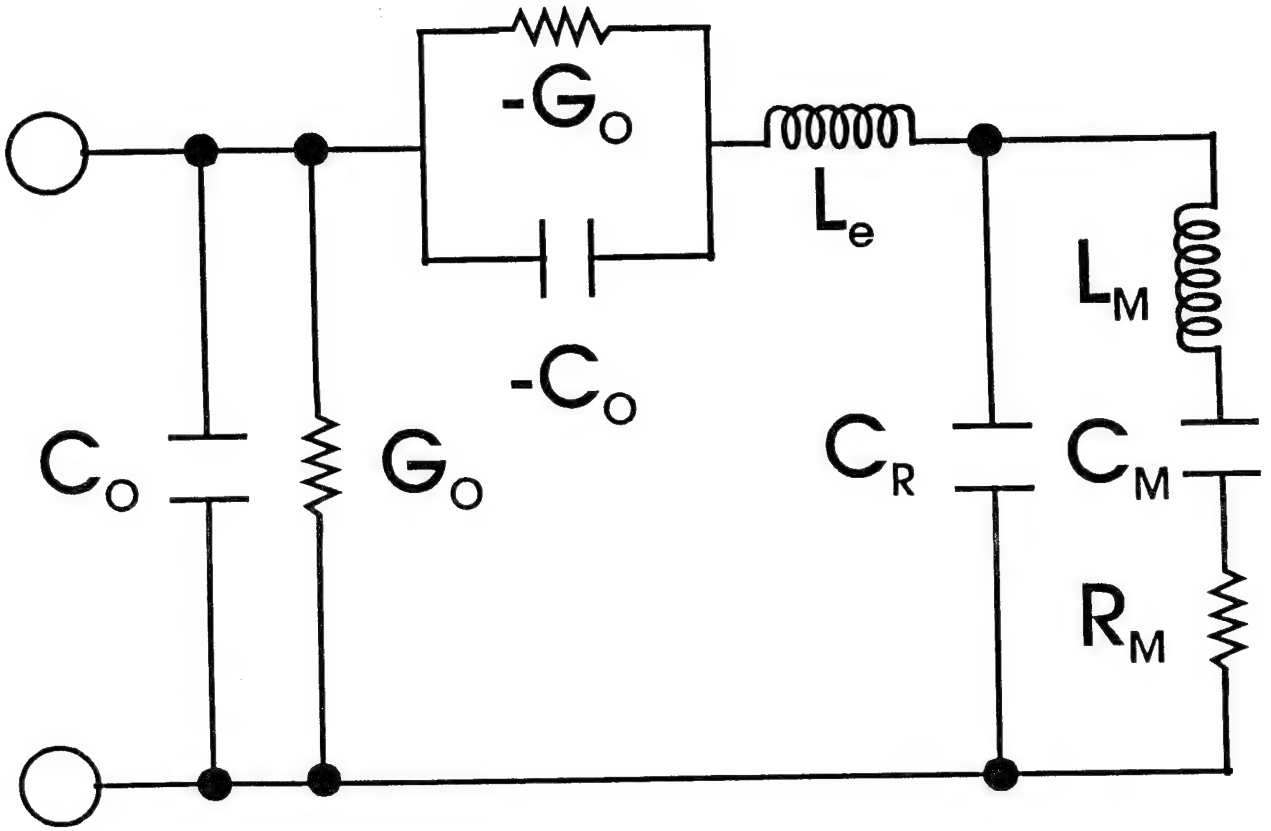

Figure 14. High frequency ceramic resonator equivalent circuit for thickness excitation. The series RLC arm represents the plate resonance at the Mth harmonic. C_R models the effect of the nonresonant modes, and is particularly important for high coupling materials. Electrode inertia is represented by L_e, while G_0 models dielectric and ohmic losses. C_0 is the limiting capacitance of the plate at very high frequencies.

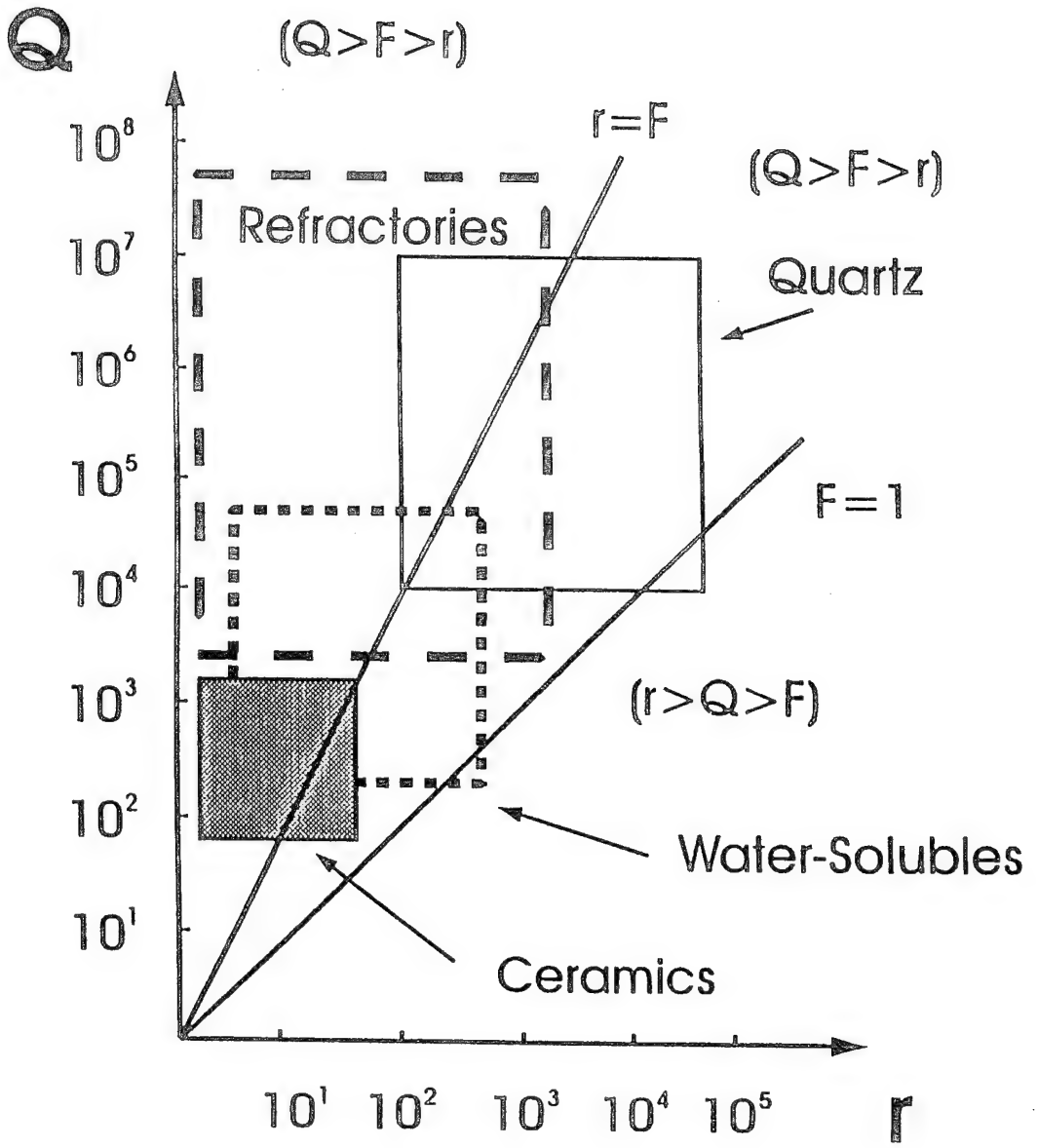

Figure 15. Sketch of quality factor, Q, vs capacitance ration, $r = C_0/C_1$, for various classes of piezoelectric materials. The quantity F in the figure is the figure of merit, $F = Q/r$. When this figure is 2 or less, the spiral of Fig. 3 ceases to intersect the G_p - f plane, and the resonance-antiresonance points are no longer real.

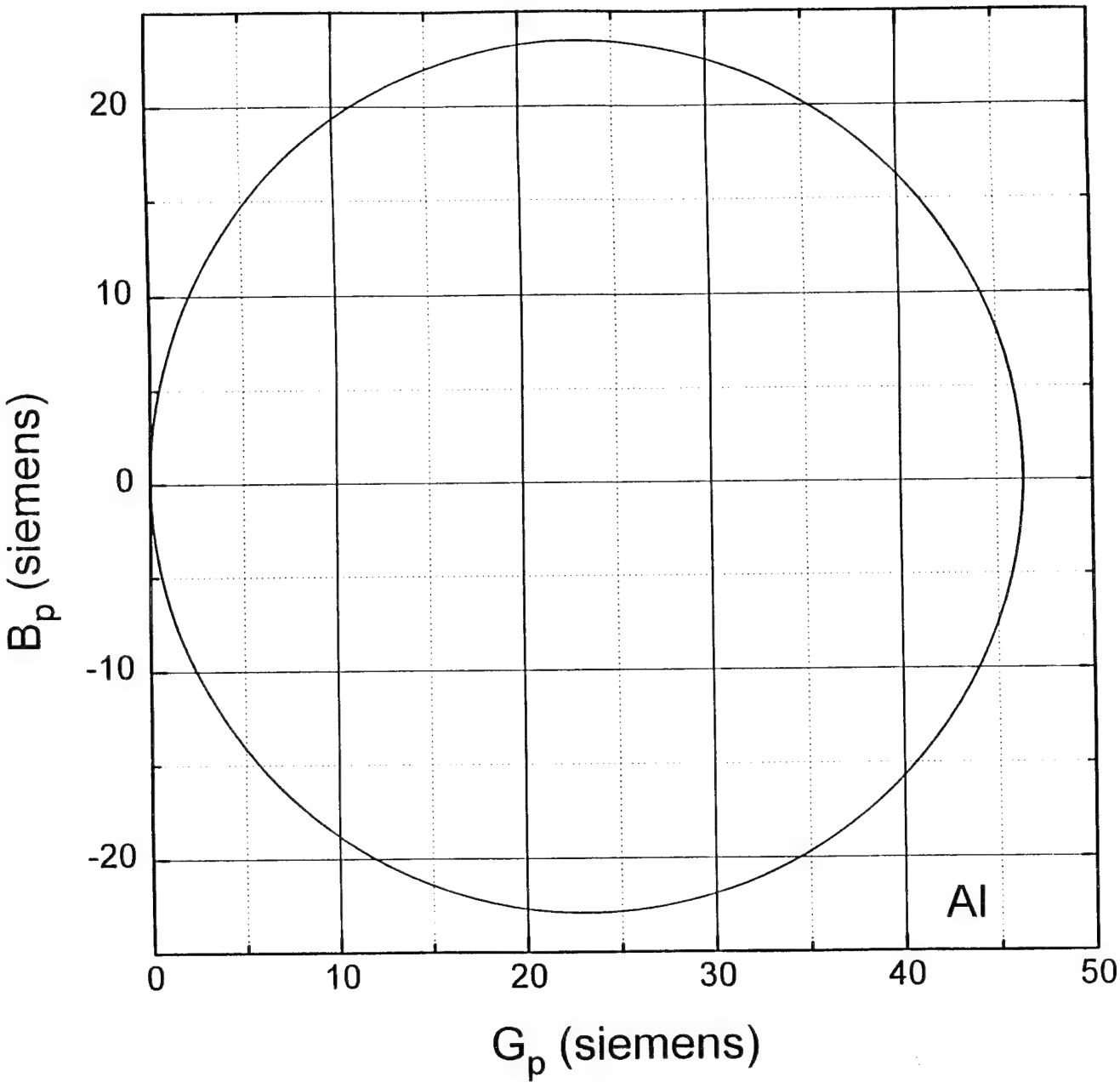

Figure 16. Network functions for the circuit of Fig. 14 with the values employed in the numerical example, and aluminum electrodes, unless otherwise noted. a). Circle diagram of input susceptance vs conductance

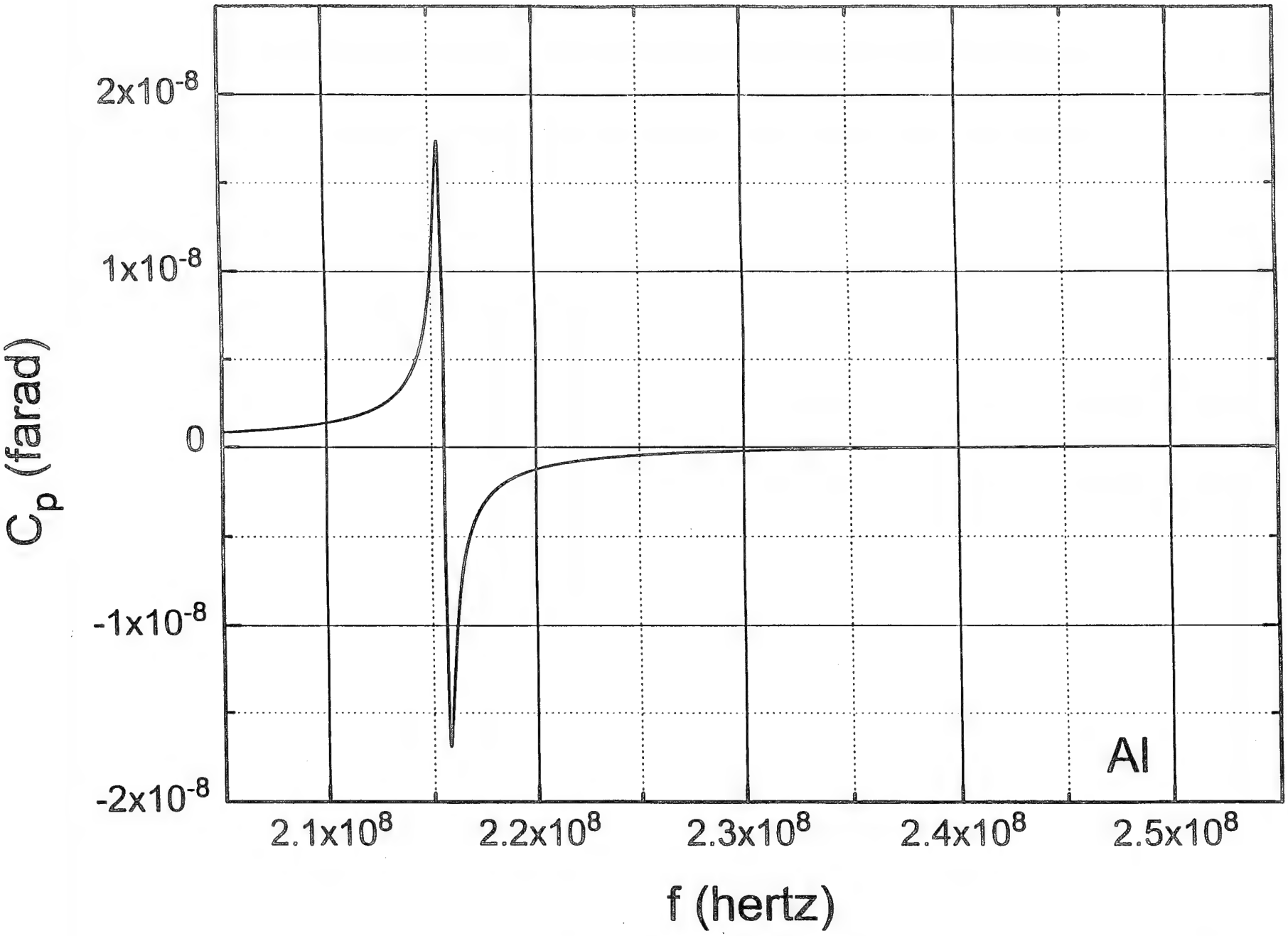

Figure 16. Network functions for the circuit of Fig. 14 with the values employed in the numerical example, and aluminum electrodes, unless otherwise noted. b). Input capacitance vs frequency

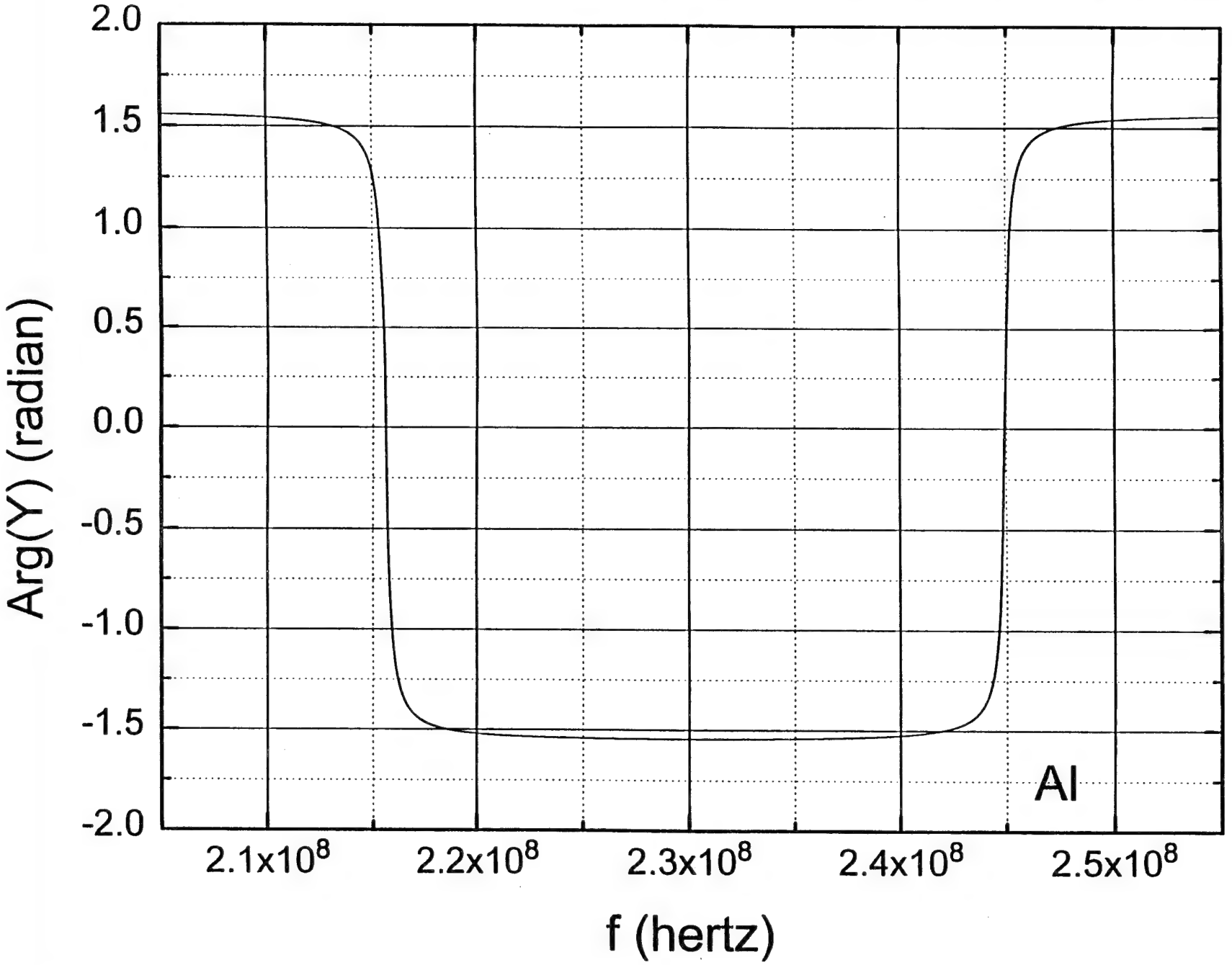

Figure 16. Network functions for the circuit of Fig. 14 with the values employed in the numerical example, and aluminum electrodes, unless otherwise noted. c). Phase angle at the input vs frequency

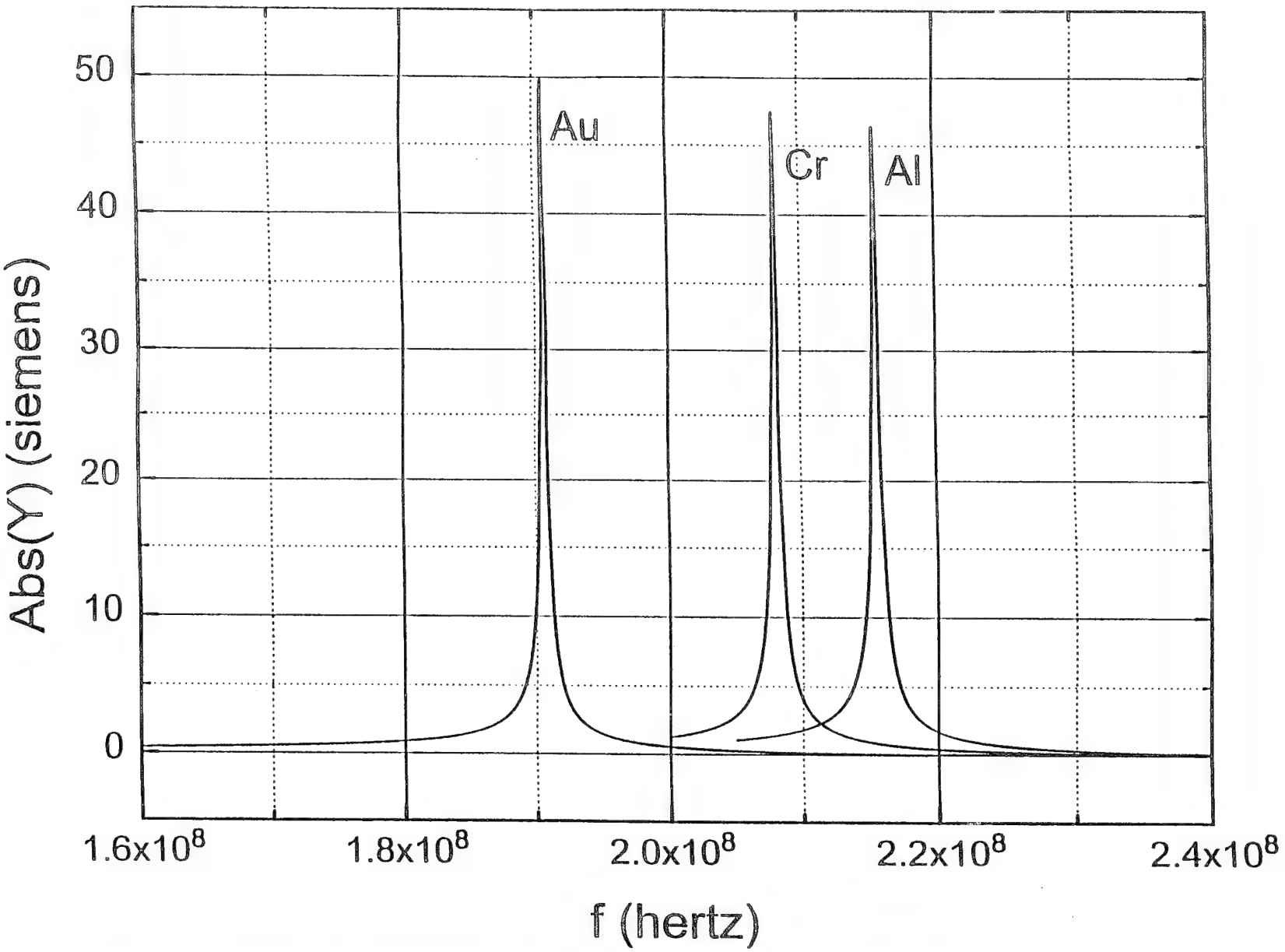

Figure 16. Network functions for the circuit of Fig. 14 with the values employed in the numerical example, and aluminum electrodes, unless otherwise noted. d). Absolute admittance versus frequency for the resonator with electrodes of aluminum, chromium, and gold. The frequency shifts are proportional to the mass densities, and must be accounted for in any accurate description of the resonator.

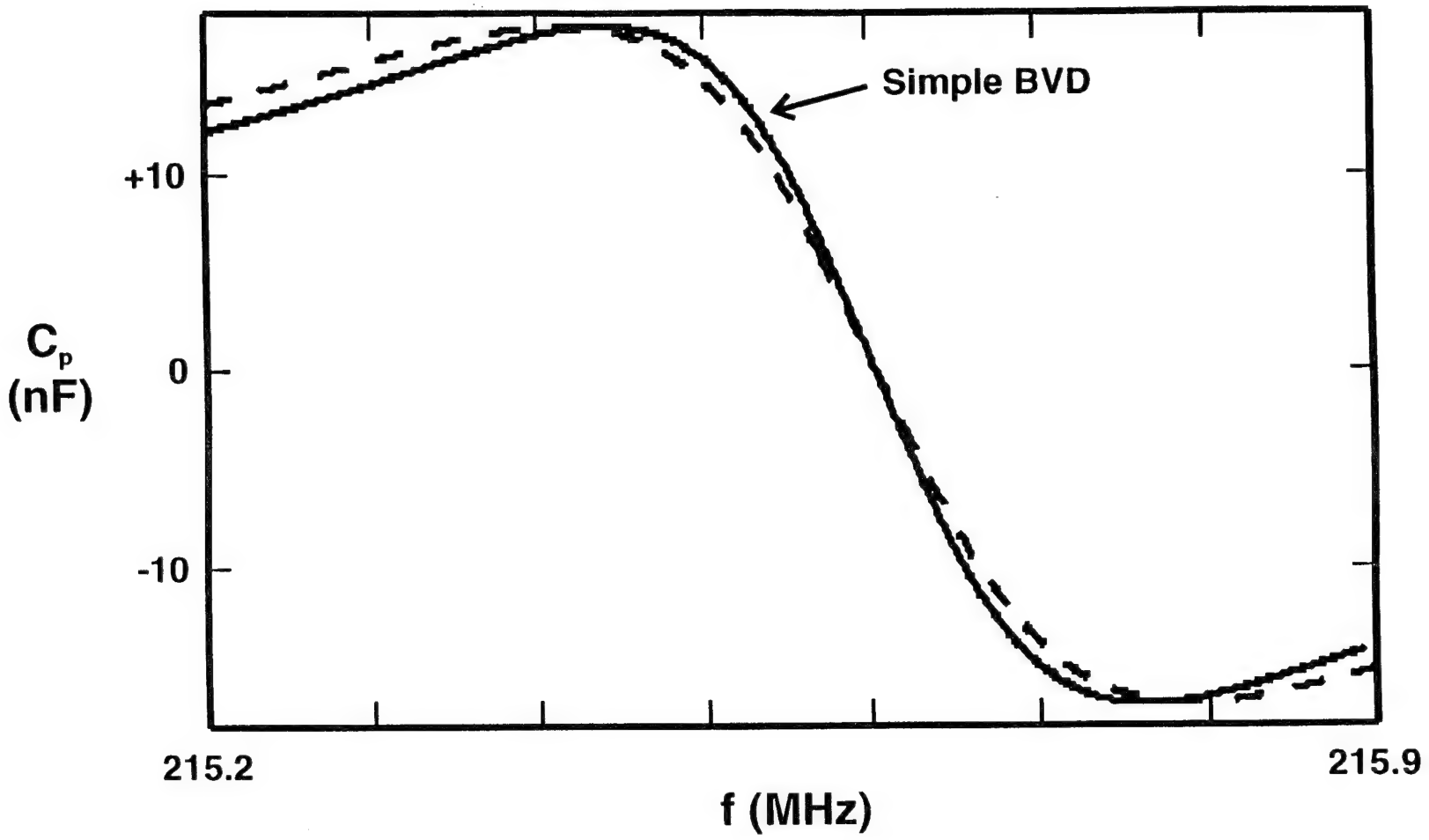

Figure 17. Network functions versus frequency in the vicinity of resonance, comparing the new, advanced lumped element circuit and a simple BVD network. a). Input capacitance. The BVD has been constructed to agree at the extrema; agreement over frequency is not adequate for characterizing modern ceramic resonators.

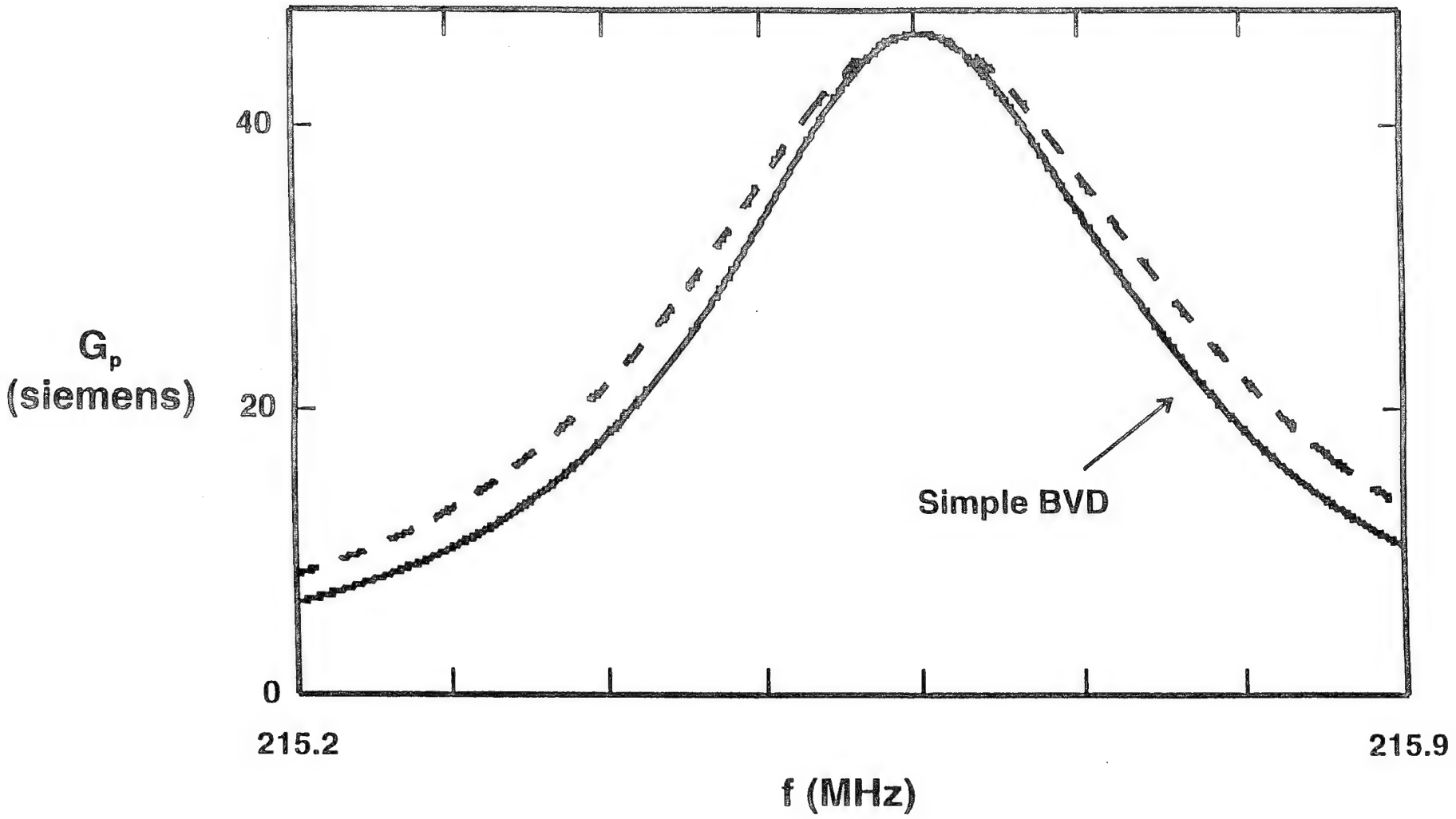

Figure 17. Network functions versus frequency in the vicinity of resonance, comparing the new, advanced lumped element circuit and a simple BVD network. b). Input conductance. The BVD has been constructed to agree at the maximum. Agreement here is likewise inadequate.

++

TABLE I. DIELECTRIC PERMITTIVITY [ε] MATRIX FOR POINT GROUP 6mm AND TRANSVERSE ISOTROPY.

ε_{11}	0	0
0	ε_{11}	0
0	0	ε_{33}

TABLE II. PIEZOELECTRIC [e] MATRIX FOR POINT GROUP 6mm AND TRANSVERSE ISOTROPY.

0	0	0	0	e_{15}	0
0	0	0	e_{15}	0	0
e_{31}	e_{31}	e_{33}	0	0	0

TABLE III. ELASTIC [c] MATRIX FOR POINT GROUP 6mm AND TRANSVERSE ISOTROPY.

c_{11}	c_{12}	c_{13}	0	0	0
c_{12}	c_{11}	c_{13}	0	0	0
c_{13}	c_{13}	c_{33}	0	0	0
0	0	0	c_{44}	0	0
0	0	0	0	c_{44}	0
0	0	0	0	0	c_{66}

$c_{66} = (c_{11} - c_{12})/2$

TABLE IV. VALUES OF PARAMETERS OF COMPLETE CIRCUIT, ALUMINUM ELECTRODES.

Parameter	Value	Frequency
$\|Y_{in}\|$= max	$\|Y_{in}\|$ = 46.385304382 S	f = 215.6001009MHz
G_p = max	G_{mx} = 46.383632396 S	f = 215.6012272MHz
B_p = max	B_{mx} = 23.470063282 S	f = 215.4137051MHz
B_p = infl	B_{infl} = 0.257642171 S	f = 215.6013114MHz
$dB_p/d\omega$ at B_p = infl	= - 39.34874044	μs/ohm
B_p = min	B_{mn} = -22.913084113 S	f = 215.7889172MHz
C_p = max	C_{mx} = 17.34048451 nF	f = 215.4135398MHz
C_p = infl	C_{infl} = 0.2201134187 nF	f = 215.6011475MHz
$dC_p/d\omega$ at C_p = infl	= - 29.04709396	fF - second
C_p = min	C_{mn} = - 16.89953315 nF	f = 215.7887560MHz
$C_p = 0$; $dC_p/d\omega < 0$		f_R = 215.6023537MHz
$C_p = 0$; $dC_p/d\omega > 0$		f_A = 244.9161150MHz

TABLE V. VALUES OF PARAMETERS OF CIRCUIT WITH $L_e = 0$, CORRESPONDING TO AN ABSENCE OF MASS LOADING.

Parameter	Value	Frequency
$\|Y_{in}\|$= max	$\|Y_{in}\|$ = 45.695069046 S	f = 220.4523222 MHz
G_p = max	G_{mx} = 45.693288121 S	f = 220.4535472 MHz
B_p = max	B_{mx} = 23.131662750 S	f = 220.2574248 MHz
B_p = infl	B_{infl} = 0.264757835 S	f = 220.4536353 MHz
$dB_p/d\omega$ at B_p = infl	= -37.063308726	μs/ohm
B_p = min	B_{mn} = -22.561117558 S	f = 220.6498443 MHz
C_p = max	C_{mx} = 16.71462358 nF	f = 220.2572478 MHz
C_p = infl	C_{infl} = 0.2206966827 nF	f = 220.4534596 MHz
$dC_p/d\omega$ at C_p = infl	= -26.75779408	fF - second
C_p = min	C_{mn} = -16.27336196 nF	f = 220.6496720 MHz
$C_p = 0$; $dC_p/d\omega < 0$		f_R = 220.4547724 MHz
$C_p = 0$; $dC_p/d\omega > 0$		f_A = 249.9119070 MHz

TABLE VI. RESONANCE AND ANTIRESONANCE FREQUENCIES FOR VARIOUS ELECTRODE MATERIALS.

Electrode material	f_R (Mhz)	f_A (Mhz)	$[(f_A - f_R)/f_1]$ (%)
massless electrode	220.4547724	249.9119070	11.78285384
Aluminum	215.6023537	244.9161150	11.72550452
Chromium	208.0472644	237.0443003	11.59881436
Gold	190.6250603	218.4866605	11.14464008

TABLE VII. VALUES OF PARAMETERS OF CIRCUIT WITHOUT $-C_0$ and $-G_0$. RESULTS APPROPRIATE TO LATERAL EXCITATION; ALUMINUM MASS LOADING.

Parameter	Value	Frequency
$\|Y_{in}\|$= max	$\|Y_{in}\|$ = 42.069823250 S	f = 244.9159862 MHz
G_p = max	G_{mx} = 42.067454235 S	f = 244.9173998 MHz
B_p = max	B_{mx} = 21.349182123 S	f = 244.7290990 MHz
B_p = infl	B_{infl} = 0.298882071 S	f = 244.9174751 MHz
$dB_p/d\omega$ at B_p = infl	= - 35.54129966	μs/ohm
B_p = min	B_{mn} = - 20.717786073 S	f = 245.1058507 MHz
C_p = max	C_{mx} = 13.88404117 nF	f = 244.7289519 MHz
C_p = infl	C_{infl} = 0.21533716 nF	f = 244.9173296 MHz
$dC_p/d\omega$ at C_p = infl	= - 23.09600438	fF - second
C_p = min	C_{mn} = - 13.45271446 nF	f = 245.1057080 MHz
$C_p = 0$; $dC_p/d\omega < 0$		f_R = 244.9188136 MHz
$C_p = 0$; $dC_p/d\omega > 0$		f_A = 268.8881905 MHz

TABLE VIII. VALUES OF PARAMETERS OF CIRCUIT WITH C_R and $L_e = 0$.

Parameter	Value	Frequency
$\|Y_{in}\|$= max	$\|Y_{in}\|$ = 41.302065813 S	f = 221.9957814 MHz
G_p = max	G_{mx} = 41.300259872 S	f = 221.9970788 MHz
B_p = max	B_{mx} = 20.923000271 S	f = 221.8009557 MHz
B_p = infl	B_{infl} = 0.254698334 S	f = 221.9971664 MHz
$dB_p/d\omega$ at B_p = infl	= - 33.49994878	μs/ohm
B_p = min	B_{mn} = - 20.376776814 S	f = 222.1933755 MHz
C_p = max	C_{mx} = 15.01346206 nF	f = 221.8007800 MHz
C_p = infl	C_{infl} = 0.2089434853 nF	f = 221.9969918 MHz
$dC_p/d\omega$ at C_p = infl	= - 24.01707857	fF - second
C_p = min	C_{mn} = - 14.59569168 nF	f = 222.1932044 MHz
$C_p = 0$; $dC_p/d\omega < 0$		f_R = 221.9983766 MHz
$C_p = 0$; $dC_p/d\omega > 0$		f_A = 249.9118350 MHz

TABLE IX. VALUES OF PARAMETERS OF CIRCUIT WITH $C_R = 0$.

Parameter	Value	Frequency
$\|Y_{in}\|$= max	$\|Y_{in}\|$ = 41.302005575 S	f = 217.5974847 MHz
G_p = max	G_{mx} = 41.300270484 S	f = 217.5987066 MHz
B_p = max	B_{mx} = 20.917603958 S	f = 217.4102764 MHz
B_p = infl	B_{infl} = 0.249734598 S	f = 217.5987887 MHz
$dB_p/d\omega$ at B_p = infl	= - 34.86793248	μs/ohm
B_p = min	B_{mn} = -20.382202679 S	f = 217.7873002 MHz
C_p = max	C_{mx} = 15.31271378 nF	f = 217.4101108 MHz
C_p = infl	C_{infl} = 0.20894304 nF	f = 217.5986246 MHz
$dC_p/d\omega$ at C_p = infl	= - 25.5031160216	fF - second
C_p = min	C_{mn} = - 14.89494338 nF	f = 217.7871392 MHz
$C_p = 0$; $dC_p/d\omega < 0$		f_R = 217.5999287 MHz
$C_p = 0$; $dC_p/d\omega > 0$		f_A = 244.9604595 MHz

TABLE X. FREQUENCIES FOR WHICH $|Y_{in}|$ = MAXIMUM.

Circuit condition	Frequency (MHz)	$\|Y_{in}\|$ (siemens)
Complete circuit	215.6001009	46.385304382
$-C_0 = -G_0 = 0$	244.9159862	42.069823250
$C_R = L_e = 0$	221.9957814	41.302065813
$L_e = 0$	220.4523222	45.695069046
$C_R = 0$	217.5974847	41.302005575

TABLE XI. FREQUENCIES FOR WHICH G_p = MAXIMUM.

Circuit condition	Frequency (MHz)	Gp (siemens)
Complete circuit	215.6012272	46.383632396
$-C_0 = -Go = 0$	244.9173998	42.067454235
$C_R = L_e = 0$	221.9970788	41.300259872
$L_e = 0$	220.4535472	45.693288121
$C_R = 0$	217.5987066	41.300270484

TABLE XII. FREQUENCIES FOR WHICH B_p = MAXIMUM.

Circuit condition	Frequency (MHz)	Bp (siemens)
Complete circuit	215.4137051	23.470063282
$-C_0 = -G_0 = 0$	244.7290990	21.349182123
$C_R = L_e = 0$	221.8009557	20.923000271
$L_e = 0$	220.2574248	23.131662750
$C_R = 0$	217.4102764	20.917603958

TABLE XIII. FREQUENCIES FOR WHICH B_p = INFLECTION POINT.

Circuit condition	Frequency (MHz)	Bp (siemens)
Complete circuit	215.6013114	0.257642171
$-C_0 = -G_0 = 0$	244.9174751	0.298882071
$C_R = L_e = 0$	221.9971664	0.254698334
$L_e = 0$	220.4536353	0.264757835
$C_R = 0$	217.5987887	0.249734598

TABLE XIV. FREQUENCIES FOR WHICH B_p = MINIMUM.

Circuit condition	Frequency (MHz)	Bp (siemens)
Complete circuit	215.7889172	-22.913084113
$-C_0 = -G_0 = 0$	245.1058507	-20.717786073
$C_R = L_e = 0$	222.1933755	-20.376776814
$L_e = 0$	220.6498443	-22.561117558
$C_R = 0$	217.7873002	-20.382202679

TABLE XV. FREQUENCIES FOR WHICH C_p = MAXIMUM.

Circuit condition	Frequency (MHz)	C_p / C_0
Complete circuit	215.4135398	88.56222937
$-C_0 = -G_0 = 0$	244.7289519	70.90930117
$C_R = L_e = 0$	221.8007800	76.67753861
$L_e = 0$	220.2572478	85.36579969
$C_R = 0$	217.4101108	78.20589265

TABLE XVI. FREQUENCIES FOR WHICH C_p = INFLECTION POINT.

Circuit condition	Frequency (MHz)	C_p / C_0
Complete circuit	215.6011475	1.124174719
$-C_0 = -G_0 = 0$	244.9173296	1.099781205
$C_R = L_e = 0$	221.9969918	1.067127068
$L_e = 0$	220.4534596	1.127153626
$C_R = 0$	217.5986246	1.067124821

TABLE XVII. FREQUENCIES FOR WHICH C_p = MINIMUM.

Circuit condition	Frequency (MHz)	C_p / C_0
Complete circuit	215.7887560	-86.31017952
$-C_0 = -G_0 = 0$	245.1057080	-68.70640684
$C_R = L_e = 0$	222.1932044	-74.54387988
$L_e = 0$	220.6496720	-83.11216527
$C_R = 0$	217.7871392	-76.07223381

TABLE XVIII. RESONANCE AND ANTIRESONANCE FREQUENCIES, ALUMINUM ELECTRODES.

Circuit condition	f_R (Mhz)	f_A (Mhz)	$[(f_A - f_R)/f_1]$ (%)
Complete circuit	215.6023537	244.9161150	11.72550452
$-C_0 = -G_0 = 0$	244.9188136	268.8881905	9.58775076
$C_R = L_e = 0$	221.9983766	249.9118350	11.16538336
$L_e = 0$	220.4547724	249.9119070	11.78285384
$C_R = 0$	217.5999287	244.9604595	10.94421232

[Tables for Al, Cr, and Au have, for the two cases each where $L_e = 0$, the same values for f_R and for f_A, as they must.]

TABLE XIX. RESONANCE AND ANTIRESONANCE FREQUENCIES, CHROMIUM ELECTRODES.

Circuit condition	f_R (Mhz)	f_A (Mhz)	$[(f_A - f_R)/f_1]$ (%)
Complete circuit	208.0472644	237.0443003	11.59881436
$-C_0 = -G_0 = 0$	237.0466749	260.9394918	9.55712676
$C_R = L_e = 0$	221.9983766	249.9118350	11.16538336
$L_e = 0$	220.4547724	249.9119070	11.78285384
$C_R = 0$	210.8100702	237.3170149	10.60277788

TABLE XX. RESONANCE AND ANTIRESONANCE FREQUENCIES, GOLD ELECTRODES.

Circuit condition	f_R (Mhz)	f_A (Mhz)	$[(f_A - f_R)/f_1]$ (%)
Complete circuit	190.6250603	218.4866605	11.14464008
$-C_0 = -G_0 = 0$	218.4883918	241.8268696	9.33539112
$C_R = L_e = 0$	221.9983766	249.9118350	11.16538336
$L_e = 0$	220.4547724	249.9119070	11.78285384
$C_R = 0$	195.2873702	219.8428424	9.82218888

TABLE XXI. SUSCEPTANCE AND CAPACITANCE SLOPES AT INFLECTION POINTS; ALUMINUM ELECTRODES.

Circuit condition	$dB_p/d\omega$	$d(C_p/C_0)/d\omega$
	(10^{-6} second/ohm)	(10^{-4} second)
Complete circuit	-39.34874044	-1.483508373
$-C_0 = -G_0 = 0$	-35.54129966	-1.179571215
$C_R = L_e = 0$	-33.49994878	-1.226612797
$L_e = 0$	-37.06330873	-1.366588053
$C_R = 0$	-34.86793248	-1.302508479

TABLE XXII. FREQUENCIES (MHz) OF ADMITTANCE MAXIMA FOR VARIOUS CIRCUIT FRAGMENTS.

Circuit conditions	Motional arm only	Motional arm & C_R	Motional & L_e, C_R	$\lvert Y_{in} \rvert_{max}$
Complete circuit	249.9	249.9	244.9	215.6
$-C_0$ & $-G_0 = 0$	249.9	249.9	244.9	244.9
$C_R = L_e = 0$	249.9			221.9
$L_e = 0$	249.9	249.9		220.4
$C_R = 0$	249.9		244.9	217.6

TABLE XXIII. VALUES OF Q' AND D_f AT f = 1 kHz.

Circuit condition	$Q' = B_p/G_p$	$D_f = 1/Q'$ (in 10^{-3})
Complete circuit	166.9988	5.98806
$-C_0 = -G_0 = 0$	136.4330	7.32960
$C_R = L_e = 0$	147.7577	6.76784
$L_e = 0$	166.9990	5.98806
$C_R = 0$	147.7577	6.76784
C_0, G_0 fragment only	108.2618	9.23687

TABLE XXIV. COMPARISON OF ADVANCED AND SIMPLE BVD CIRCUITS.

Quantity	Advanced Circuit	Five-Element BVD
Capacitance ratio, r	4.74	3.84
Surge impedance, z_1	15.42 ohm	14.49 ohm
Quality factor, Q	637.	672.
Figure of merit, F	134.	175.
Figure of excellence, E	85,400.	117,550.
Motional time constant, τ_1	1.000 ps	1.099 ps
$d(C_p/C_0)/d\Omega\lvert_{infl.}$	$-2.010\ 10^5$	$-2.352\ 10^5$

++

ARMY RESEARCH LABORATORY
PHYSICAL SCIENCES DIRECTORATE
MANDATORY DISTRIBUTION LIST

Defense Technical Information Center*
ATTN: DTIC-OCC
8725 John J. Kingman Rd, STE 0944
Fort Belvoir, VA 22060-6218
(*Note: Two DTIC copies will be sent from STINFO office, Ft Monmouth, NJ)

Director
US Army Material Systems Analysis Actv
ATTN: DRXSY-MP
(1) Aberdeen Proving Ground, MD 21005

Commander, AMC
ATTN: AMCDE-SC
5001 Eisenhower Ave.
(1) Alexandria, VA 22333-0001

Director
Army Research Laboratory
ATTN: AMSRL-D (John W. Lyons)
2800 Powder Mill Road
(1) Adelphi, MD 20783-1197

Director
Army Research Laboratory
ATTN: AMSRL-DD (COL Thomas A. Dunn)
2800 Powder Mill Road
(1) Adelphi, MD 20783-1197

Director
Army Research Laboratory
2800 Powder Mill Road
Adelphi, MD 20783-1197
(1) AMSRL-OP-SD-TA (ARL Records Mgt)
(1) AMSRL-OP-SD-TL (ARL Tech Library)
(1) AMSRL-OP-SD-TP (ARL Tech Publ Br)

Directorate Executive
Army Research Laboratory
Physical Sciences Directorate
Fort Monmouth, NJ 07703-5601
(1) AMSRL-PS
(1) AMSRL-PS-T (M. Hayes)
(1) AMSRL-OP-FM-RM
(22) Originating Office

Advisory Group on Electron Devices
ATTN: Documents
Crystal Square 4
1745 Jefferson Davis Highway, Suite 500
(2) Arlington, VA 22202

Commander, CECOM
R&D Technical Library
Fort Monmouth, NJ 07703-5703
(1) AMSEL-IM-BM-I-L-R (Tech Library)
(3) AMSEL-IM-BM-I-L-R (STINFO Ofc)

Deputy for Science & Technology
Office, Asst Sec Army (R&D)
(1) Washington, DC 20310

HQDA (DAMA-ARZ-D/
Dr. F.D. Verderame)
(1) Washington, DC 20310

Director
Naval Research Laboratory
ATTN: Code 2627
(1) Washington, DC 20375-5000

USAF Rome Laboratory
Technical Library, FL2810
ATTN: Documents Library
Corridor W, STE 262, RL/SUL
26 Electronics Parkway, Bldg 106
Griffiss Air Force Base
(1) NY 13441-4514

Dir, ARL Battlefield
Environment Directorate
ATTN: AMSRL-BE
White Sands Missile Range
(1) NM 88002-5501

Dir, ARL Sensors, Signatures,
Signal & Information Processing
Directorate (S3I)
ATTN: AMSRL-SS
2800 Powder Mill Road
(1) Adelphi, MD 20783-1197

Dir, CECOM Night Vision/
Electronic Sensors Directorate
ATTN: AMSEL-RD-NV-D
(1) Fort Belvoir, VA 22060-5806

Dir, CECOM Intelligence and
Electronic Warfare Directorate
ATTN: AMSEL-RD-IEW-D
Vint Hill Farms Station
(1) Warrenton, VA 22186-5100

Cdr, Marine Corps Liaison Office
ATTN: AMSEL-LN-MC
(1) Fort Monmouth, NJ 07703-5033